

Chapter 3

Results and Discussion

3.1 CNTs Grown Using Multilayer Catalysts at Low Temperatures

3.1.1 Effect of interlayer (Exp. A)

It is generally believed that the formation of catalyst nanoparticles is necessary before CNT growth. In order to form these nanoparticles of catalyst, we proceeded a procedure before CNT growth— pretreatment. The pretreatment method balances the surface energy (catalyst/gas), interface energy (catalyst/substrate), and interior energy (body free energy) of catalyst's nanofilm at designated temperature, and then achieves the purpose of nanoparticles' formation. The nanoparticles can not only help the CNT growth have better quality but also control the size and morphology of CNTs. Therefore, the formation of nanoparticles plays an important role in CNT synthesis for device application.

The formation of nanoparticles has two important purposes. One is lower melting point as catalyst film thickness decreases [47]. In the Fig. 1-7, nanoparticle indeed had the lowest melting point (1057K) compared to nanowire (1315K) and nanofilm (1536K) as the size is 2nm. The other is high activity which decomposes the hydrocarbon gases because of the nano-phenomenon as the catalyst film thickness decreases. Generally, the smaller catalyst particles have higher surface energies and thus promote nucleation and growth processes of CNTs.

From the Fig. 3-1, we tried to find out if the particles are more uniform by using the specified interlayer with suitable surface energy. First, the thickness of Co and interlayer was 20A and the thickness of Al was 100A. Generally, We desired to setup without interlayer model referring to Fig. 3-1(a). Growth condition in Fig.3-1(b) and Fig.3-2(a),(b) showed the morphology after CNTs growth via Thermal-CVD. We could identified the obvious characteristic when some interlayer was deposited below catalyst, others were contrary. The field emission measurements (Fig.2-10) were done when anode applied 1000V, whose spacer was 160 μ m, and 25 dies on sample whose dimension was 100 μ m².The electric characteristics were shown in Fig.3-4 (a) & (b) , and Table. 3-1, 20A Cr and 20A Ti both presented higher current density (12.8 mA/cm²) than other interlayer metals. Considering the fabrication variation, we changed \pm 50% thickness for investigation, as shown in Fig.3-5 (a) & (b), the results were the same as the thickness was 20 A.

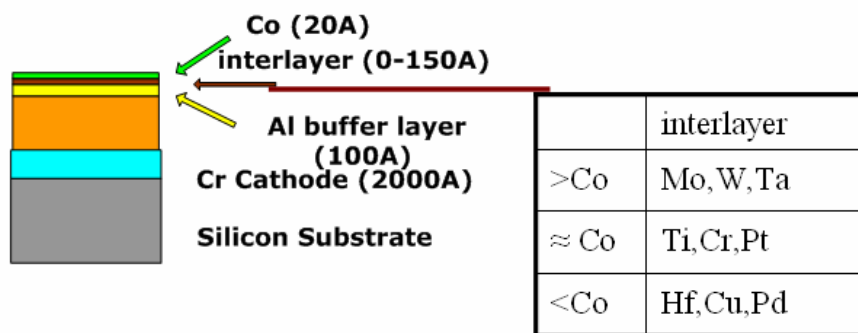
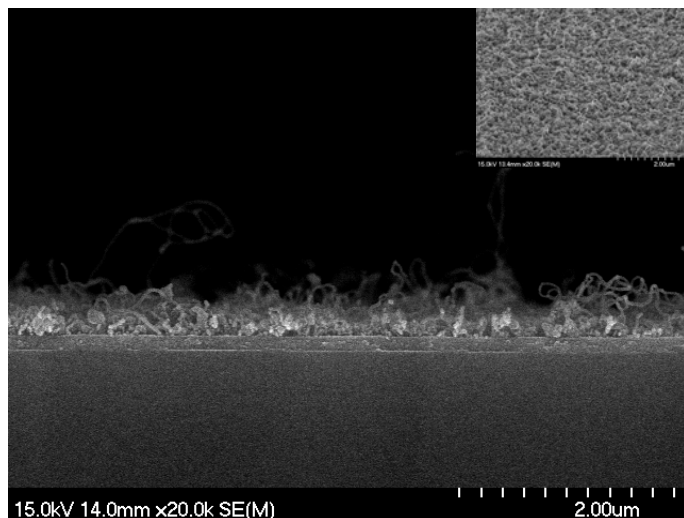
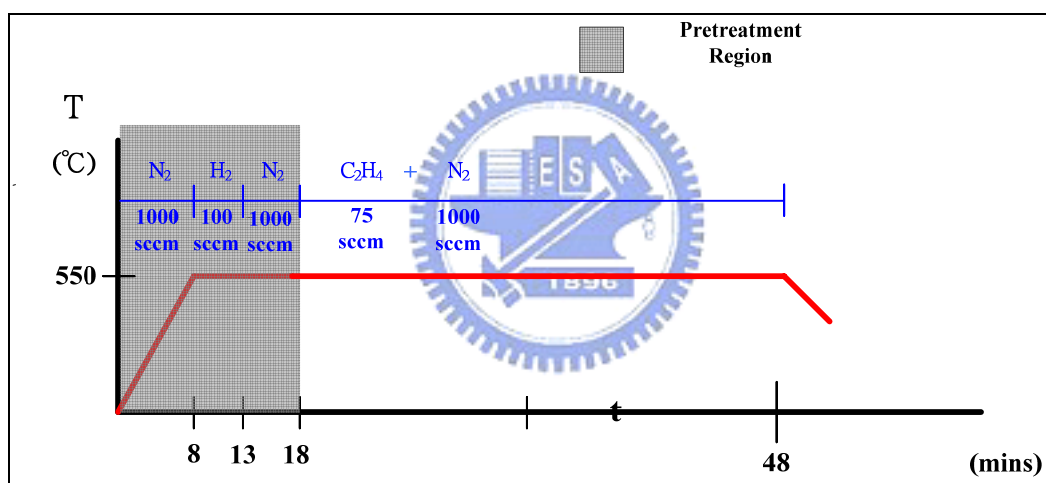


Fig. 3-1 The Surface energy of interlayer Diagram.

20Co/100Al



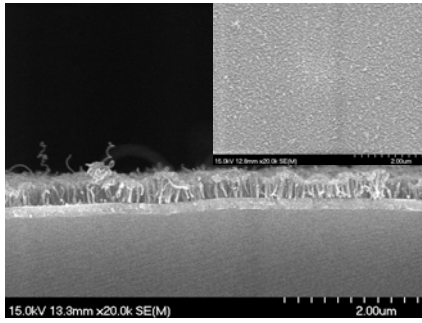
(a)



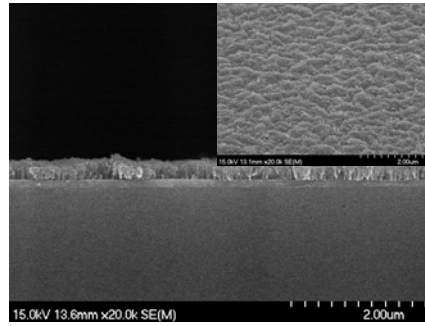
(b)

Fig. 3-2 (a) The SEM cross-section images of CNT growth without interlayer and image represents the top view image of, (b) which growth condition.

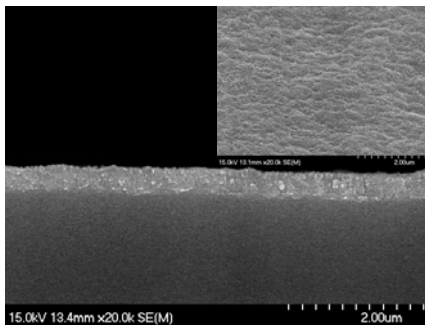
W_20



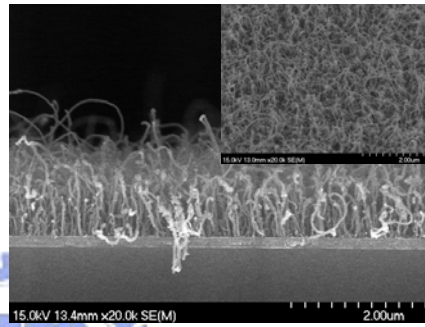
Mo_20



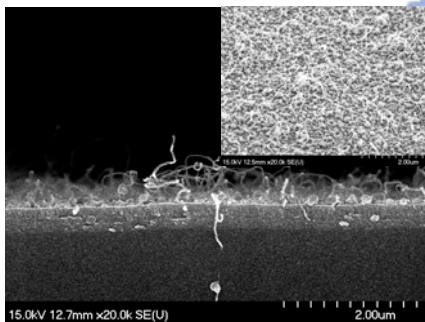
Pt_20



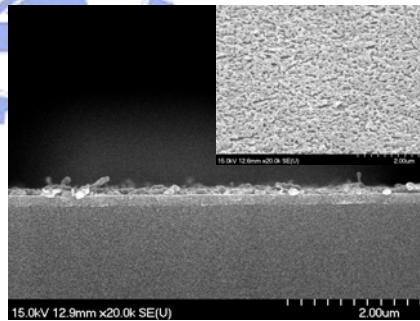
Cr_20



Hf_20



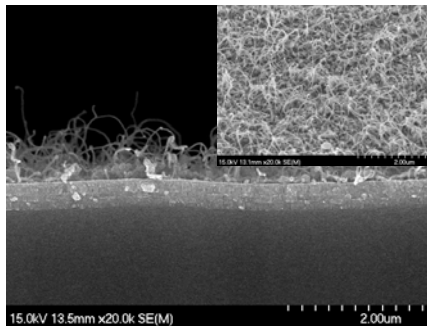
Pd_20



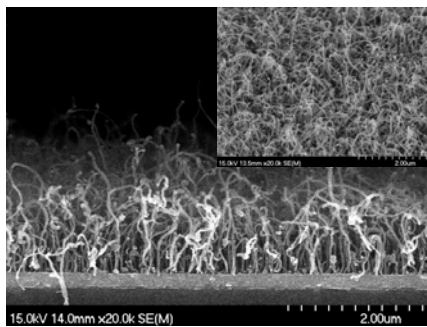
(a)

Fig. 3-3 The SEM cross-section images of CNT growth with interlayer of (a) W 20 A, Mo 20 A, Pt 20 A, Cr 20 A, Hf 20 A, Pd 20 A and image represents the top view image of, (b) which Ta 20 A, Ti 20 A, and Cu 20 A.

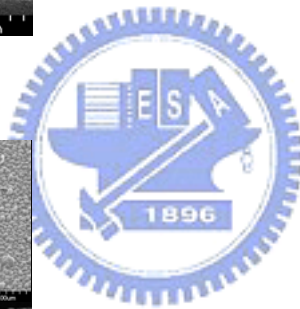
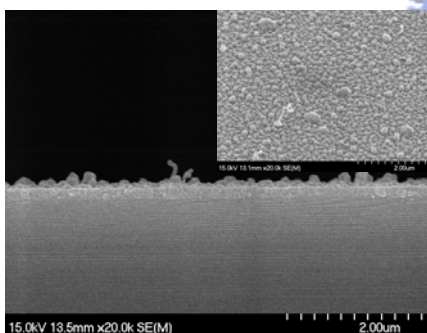
Ta_20



Ti_20

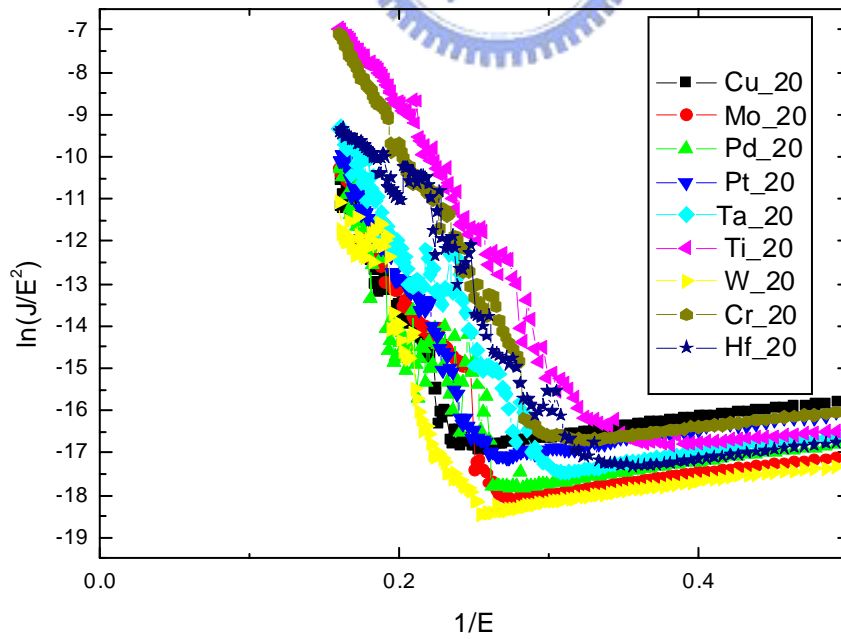
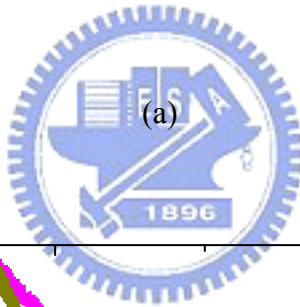
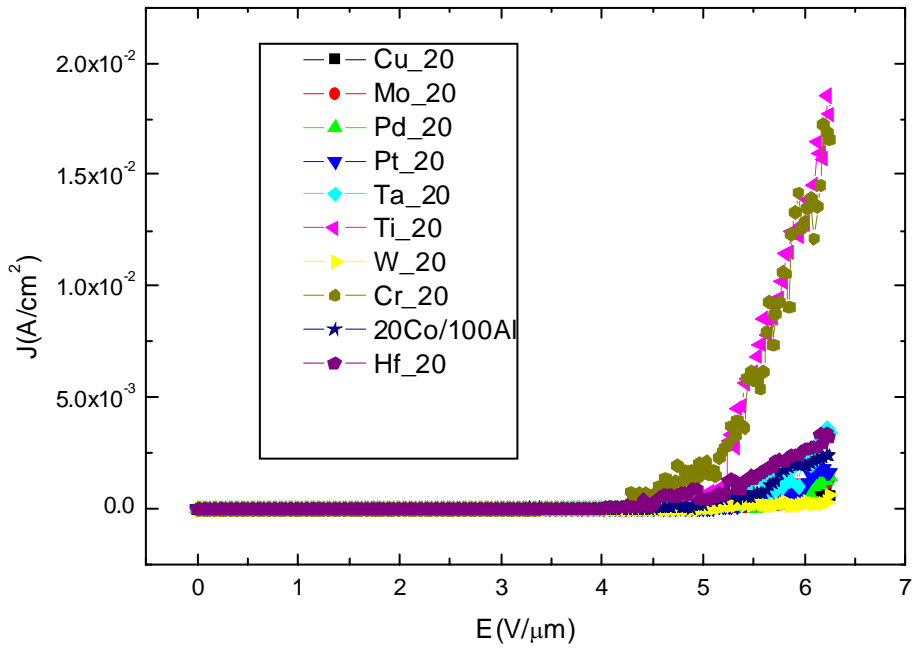


Cu_20



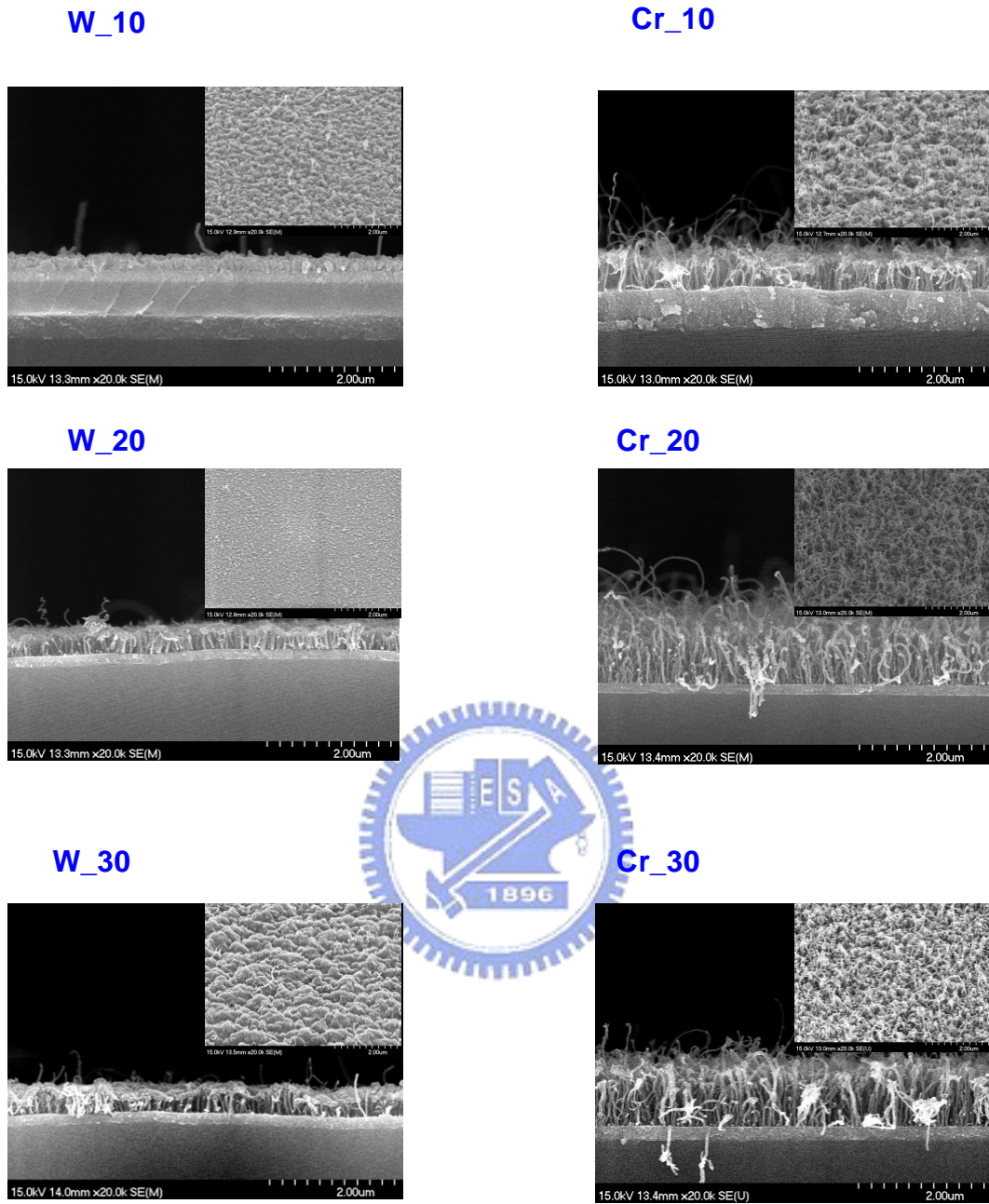
(b)

Fig. 3-3 The SEM cross-section images of CNT growth with interlayer of (a) W 20 A, Mo 20 A, Pt 20 A, Cr 20 A, Hf 20 A, Pd 20 A and image represents the top view image of, (b) which Ta 20 A, Ti 20 A, and Cu 20 A.



(b)

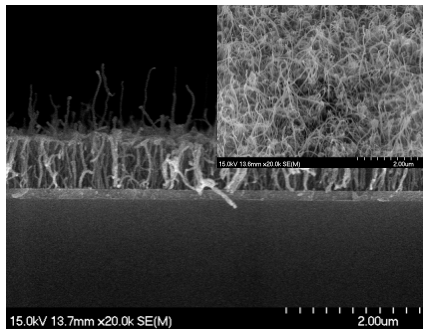
Fig. 3-4 (a) I-V plot in the Exp. A and (b) F-N plot in the Exp. A (Effect of interlayer)



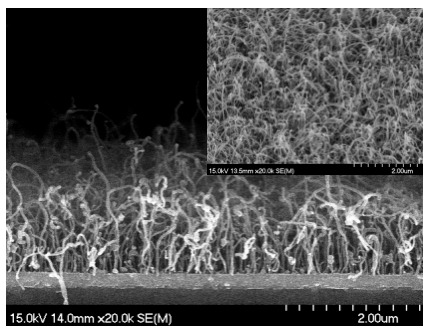
(a)

Fig. 3-5 The SEM cross-section images of CNT growth with interlayer of (a) W 10 A, W 20 A, W 30 A, Cr 10 A, Cr 20 A, Cr 30 A and image represents the top view image of, (b) which Ti 10 A, Ti 20 A, and Ti 30 A.

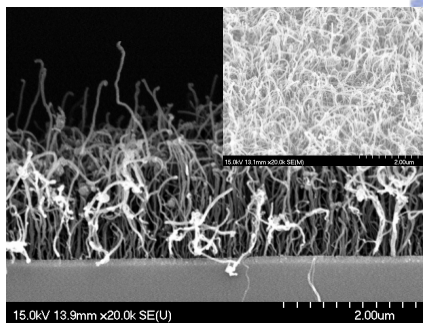
Ti_10



Ti_20



Ti_30



(b)

Fig. 3-5 The SEM cross-section images of CNT growth with interlayer of (a) W 10 A, W 20 A, W 30 A, Cr 10 A, Cr 20 A, Cr 30 A and image represents the top view image of, (b) which Ti 10 A, Ti 20 A, and Ti 30 A.

Table 3-1 Field emission characteristics in Exp.A (Effect of interlayer)

	20Co/100Al	Cu_20	Mo_20	Pd_20	Pt_20	Ta_20	Ti_20	W_20	Cr_20	Hf_20
Turn on Field (V/um)@ (J=10uA/cm2)	4.375	4.625	4.375	4.93	4.43	4.03	4.375	4.78	3.718	3.9
Anode Current (mA/cm ²)@ (E≈6 V/um)	1.95	0.596	0.98	0.48	0.98	2.35	12.8	0.23	12.8	2.64

From above, we found that four interlayer metals were helpful to CNTs growth,

So we decided to increased the thickness of chosen interlayer from 20A to 50 A. As shown in Fig.2-7(a), Fig.3-6 showed chosen Cr and Ti apparently had better morphology than others. The same results were demonstrated in the electric characteristics, in Fig.3-7 (a) & (b)).And the detail anode current density was listed in Table.3-2. Furthermore, we investigated the effect of interlayer on the graphite crystallization by Raman analysis (Fig. 3-8 (a)). The G peak and D peak were located on 1590 cm⁻¹ and 1330 cm⁻¹. The results showed that interlayer wouldn't affect the graphite crystallization of CNT growth and I_G/I_D ratio is related to anode current density (Fig. 3-8 (b)),which proves that proof Cr, Ti as interlayer would helps to CNTs growth.

Table 3-2 Field emission characteristics in Exp.A(Effect of interlayer)

	20Co/100Al	Cr_20	Cr_50	Ti_20	Ti_50	Hf_20	Hf_50	Ta_20	Ta_50
Turn on Field (V/um)@ (J=10uA/cm2)	4.375	3.718	4.59	4.375	3.5	3.9	4.875	4.03	4.9
Anode Current (mA/cm ²)@ (E≈6 V/um)	1.95	12.8	14.28	12.8	19	2.64	0.22	2.35	0.374

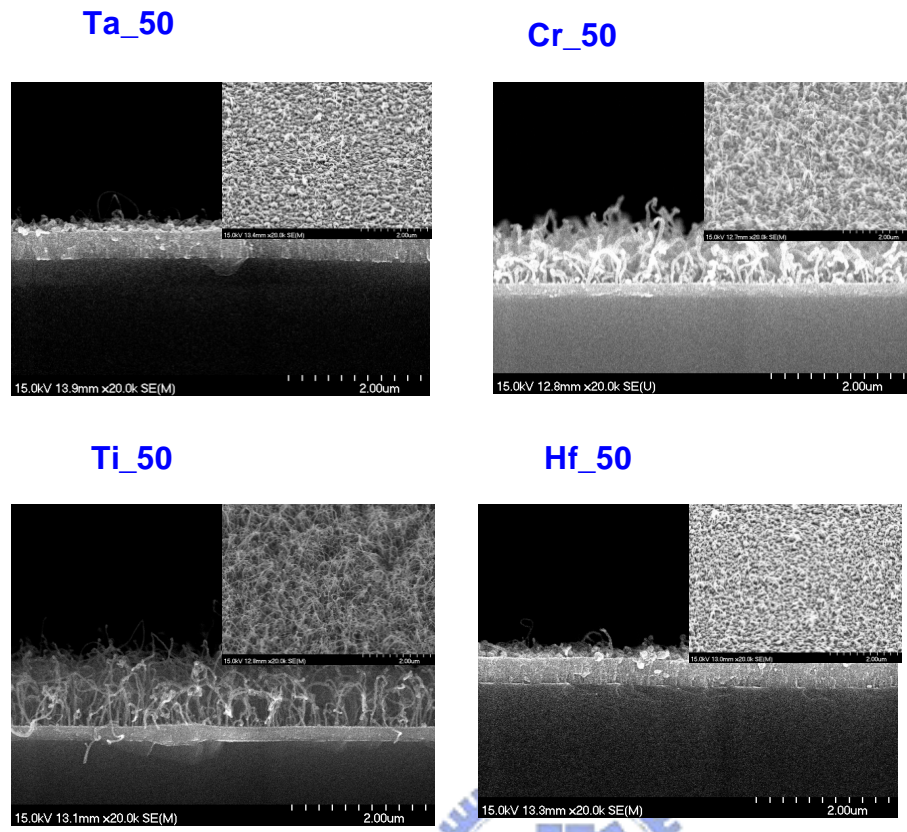
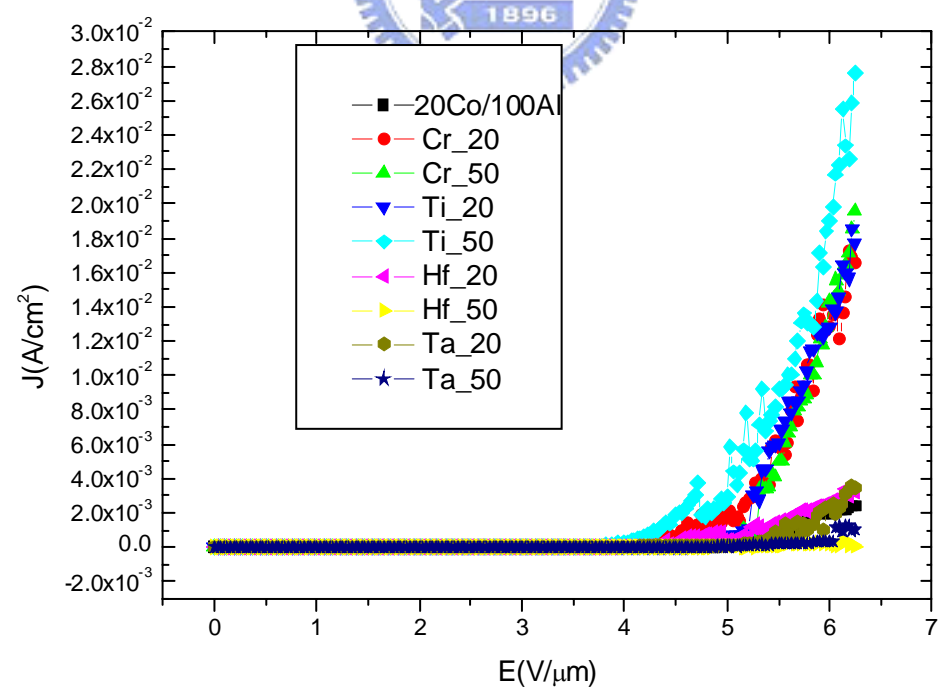
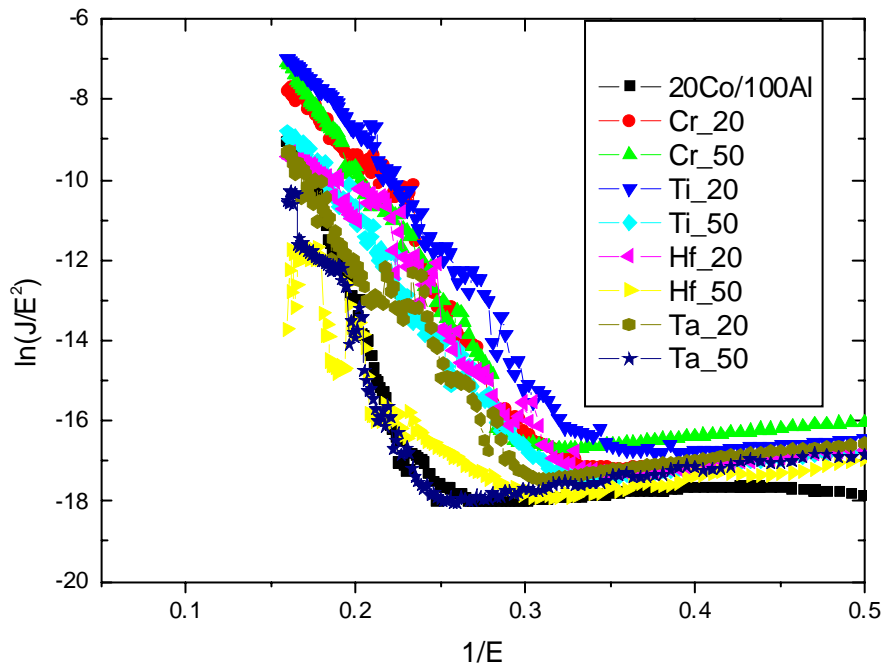


Fig. 3-6 The SEM cross-section images of CNT growth with interlayer of Ta 50 A, Cr 50 A, Ti 50 A, and Cr 50 A and image represents the top view image .



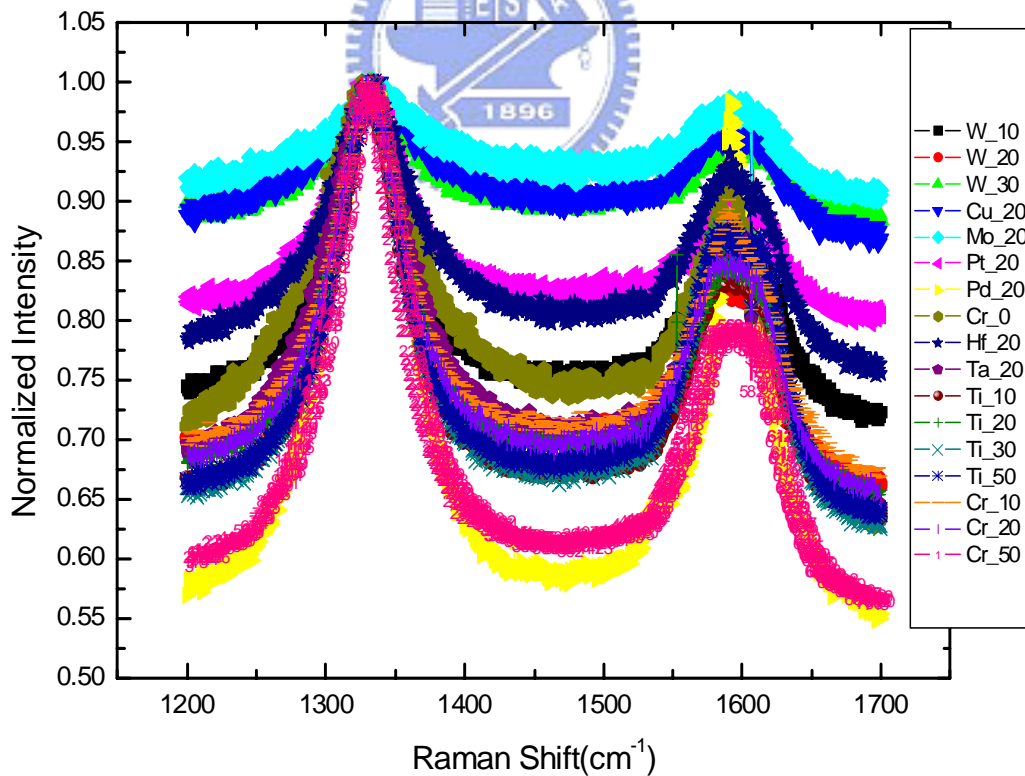
(a)

Fig. 3-7 (a) I-V plot in the Exp. A and (b) F-N plot in the Exp. A (Effect of interlayer)



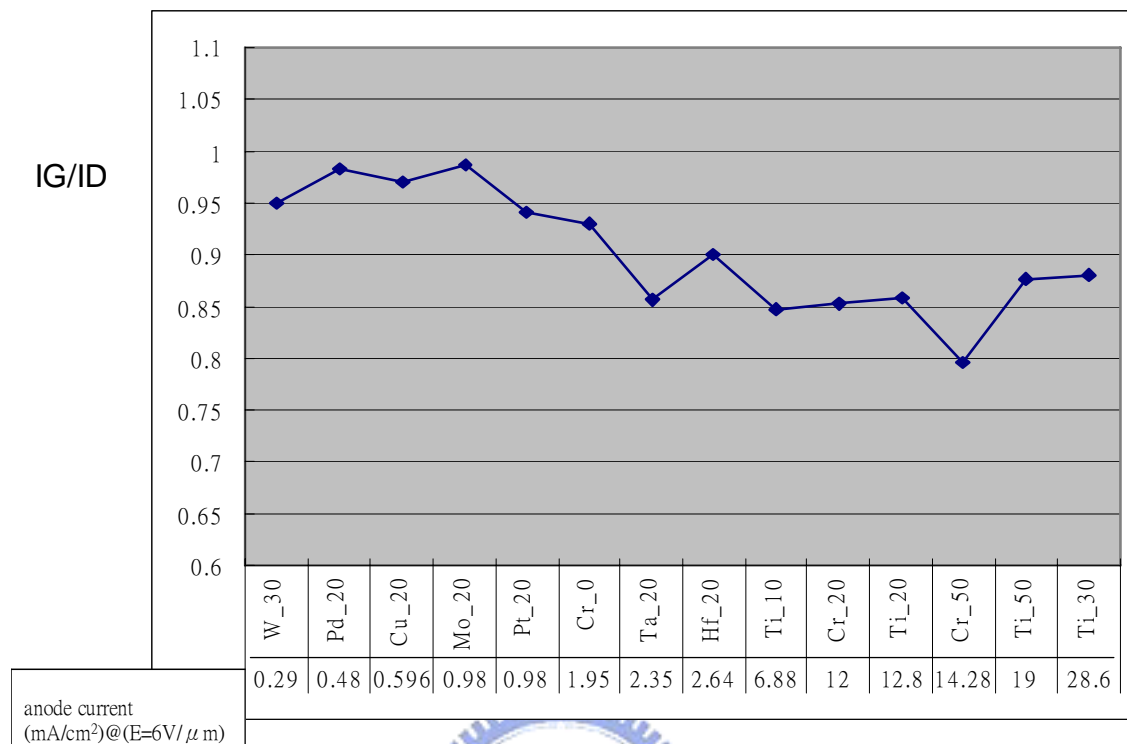
(b)

Fig. 3-7 (a) I-V plot in the Exp. A and (b) F-N plot in the Exp. A (Effect of interlayer)



(a)

Fig. 3-8 Raman analysis in Exp. A ; (a) G peak at 1590 cm^{-1} and D peak at 1330 cm^{-1} , (b) IG/ID ration vs. anode current density .



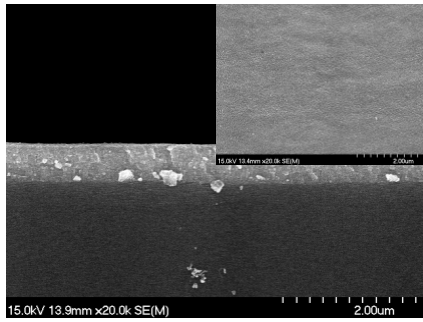
(b)
Fig. 3-8 Raman analysis in Exp. A ; (a) G peak at 1590 cm⁻¹ and D peak at 1330 cm⁻¹, (b) IG/ID ration vs. anode current density .

3.1.2 Effect of heat from formation carbide (Exp. B)

According to the Exp.A, we found something interesting. When interlayer thickness was increased, CNTs growth seems to change depending on its. So, we decided to add the Cr, Ti thickness to observe the CNTs growth morphology, as shown in Fig.2-7 (c).

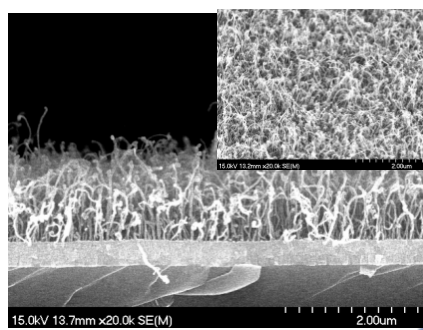
In Fig.3-9 (a), Cr interlayer was added thickness to 100 Å, and the Ti interlayer was added thickness to 100 Å, and 150 Å. The results were demonstrated in the electric characteristics in Fig.3-10 (a) - (d).And the detail anode current density was listed in Table.3-3 and Table.3-4.

Cr_100

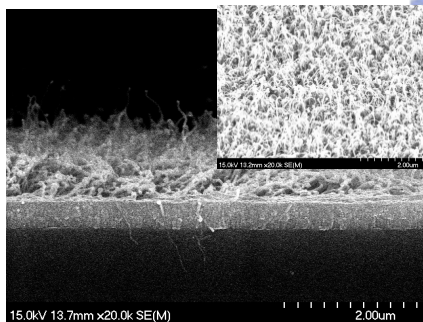


(a)

Ti_100

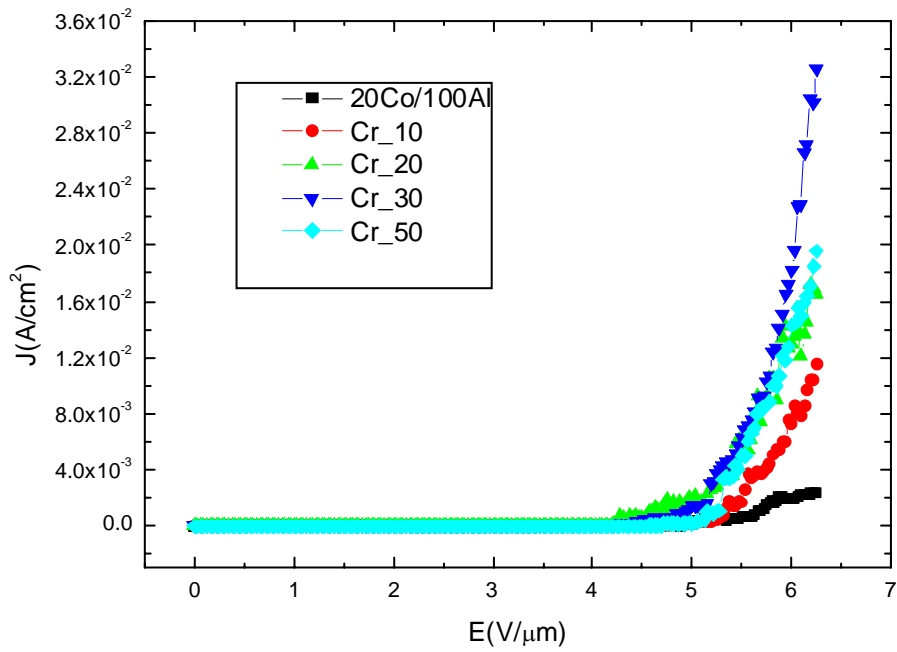


Ti_150

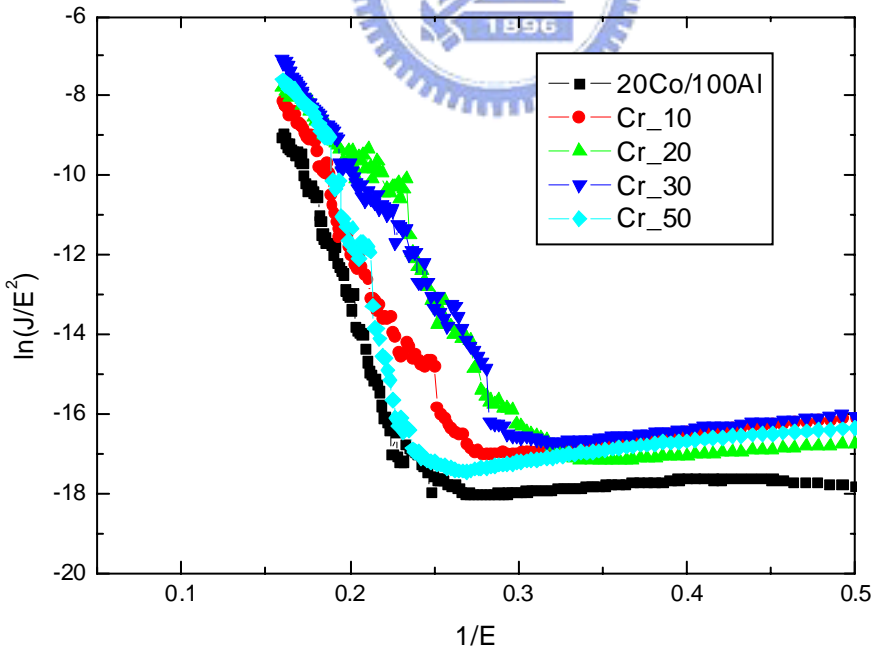


(b)

Fig. 3-9 The SEM cross-section images of CNT growth with interlayer of (a) Cr 100 A , (b) Ti 100 A, and Ti 150 A .by which image represents the top view .



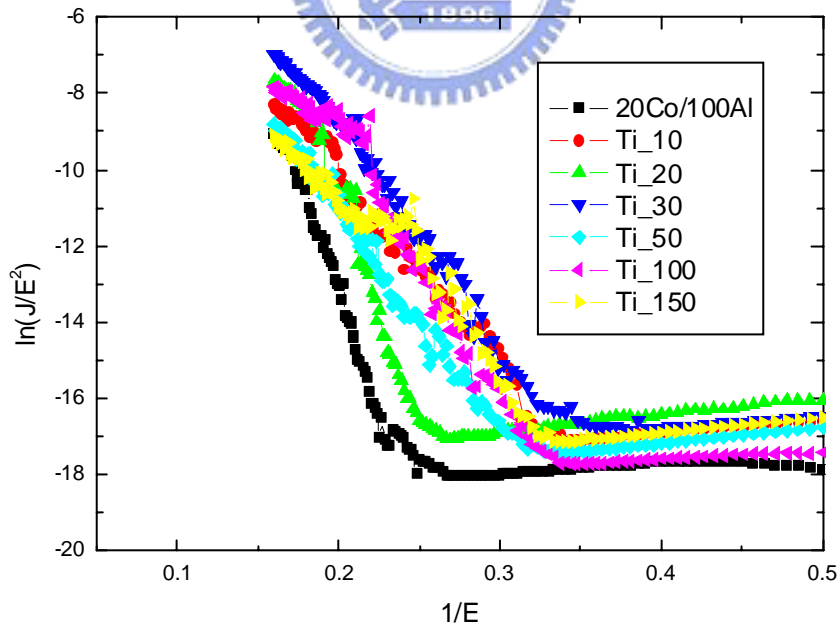
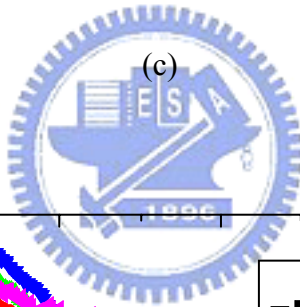
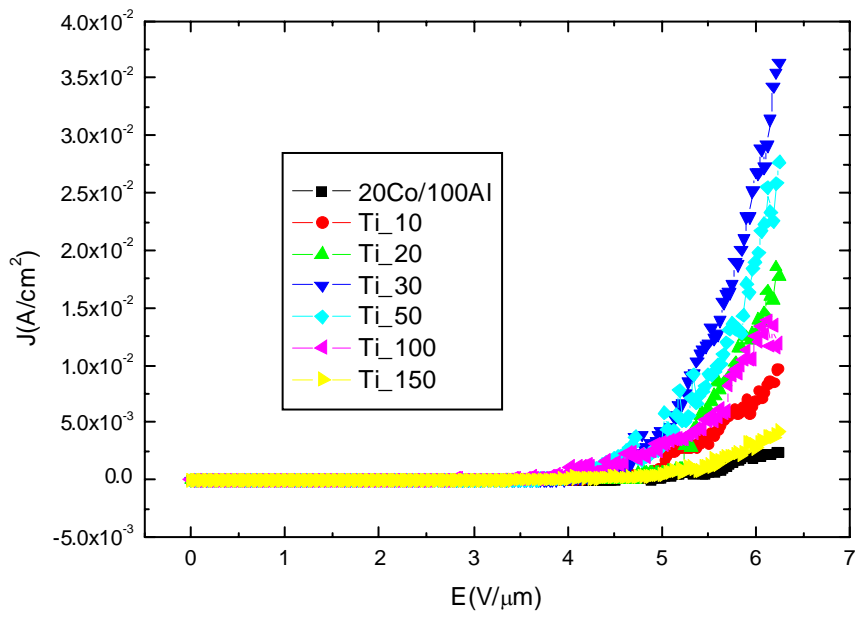
(a)



(b)

Fig. 3-10 (a), (c) I-V plot in the Exp. B and (b),(d) F-N plot in the Exp. B

(Effect of heat from formation carbide)



(d)

Fig. 3-10 (a), (c) I-V plot in the Exp. B and (b),(d) F-N plot in the Exp. B

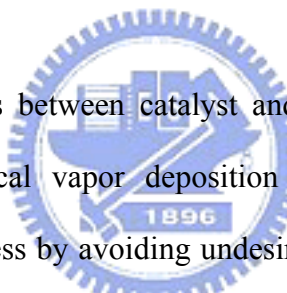
(Effect of heat from formation carbide)

Table 3-3 Field emission characteristics in Exp.B

	20Co/100Al	Cr_10	Cr_20	Cr_30	Cr_50	Cr_100
Turn on Field (V/um)@ (J=10uA/cm ²)	4.375	4.25	3.718	3.71	4.59	N.A
Anode Current (mA/cm ²)@ (E≈6 V/um)	1.95	7.28	12.8	18.24	14.28	N.A

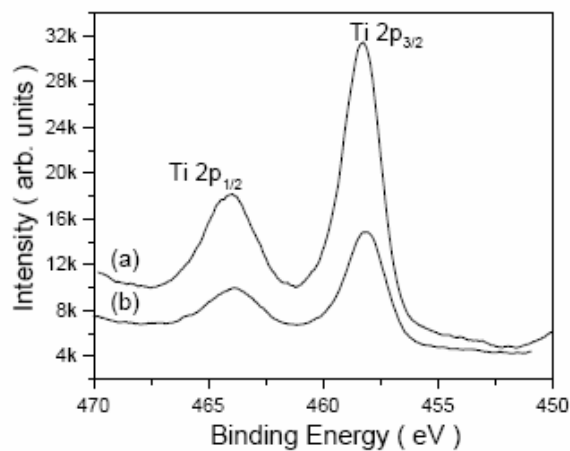
Table 3-4 Field emission characteristics in Exp.B

	20Co/100Al	Ti_10	Ti_20	Ti_30	Ti_50	Ti_100	Ti_150
Turn on Field (V/um)@ (J=10uA/cm ²)	4.375	3.625	4.375	3.5	3.5	3.125	3.56
Anode Current (mA/cm ²)@ (E≈6 V/um)	1.95	6.88	12.8	28.6	19	12.56	2.78



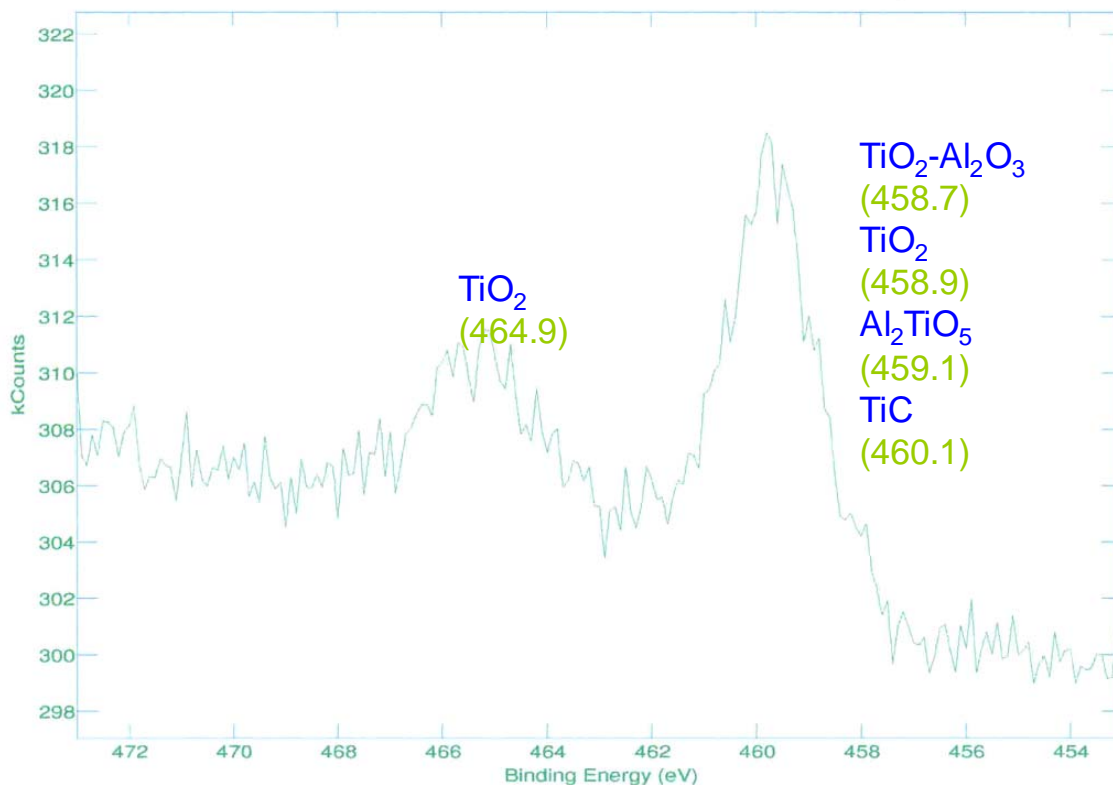
The use of buffer layers between catalyst and silicon substrate in growth of carbon nanotubes by chemical vapor deposition (CVD) can both increase the efficiency of the growth process by avoiding undesired chemical interaction between catalyst and substrate, and alter the catalyst-support interaction, therefore it can modify the characteristics and growth rate of CNTs. To sum up, using good buffer layers can effectively make catalyst films form the catalyst particles without merging together and control the CNT density as its thickness increases. In the paper surveys, the comparative efficiency of buffer layers of Al, Al₂O₃, TiN and TiO₂ in the CVD growth of CNTs was investigated. With in situ X-ray photoelectron spectroscopy (XPS) analysis(Fig.3-11(b)), Al₂O₃ and TiO₂ ayers was observed in the experiment on CNT growth, which promoted formation of nanotubes. Therefore, P. Oelhafen et al., who investigated that in the pretreatment pure Al buffer layer could transform Al into Al₂O₃ from XPS analysis and enhanced the CNT growth [48]. In Taek Han et al.'s study, spherical Al₂O₃ particles were formed during the heating prior to the CNT

growth, preventing catalyst clusters from agglomerating, which subsequently resulted in the formation of thin CNTs [49].



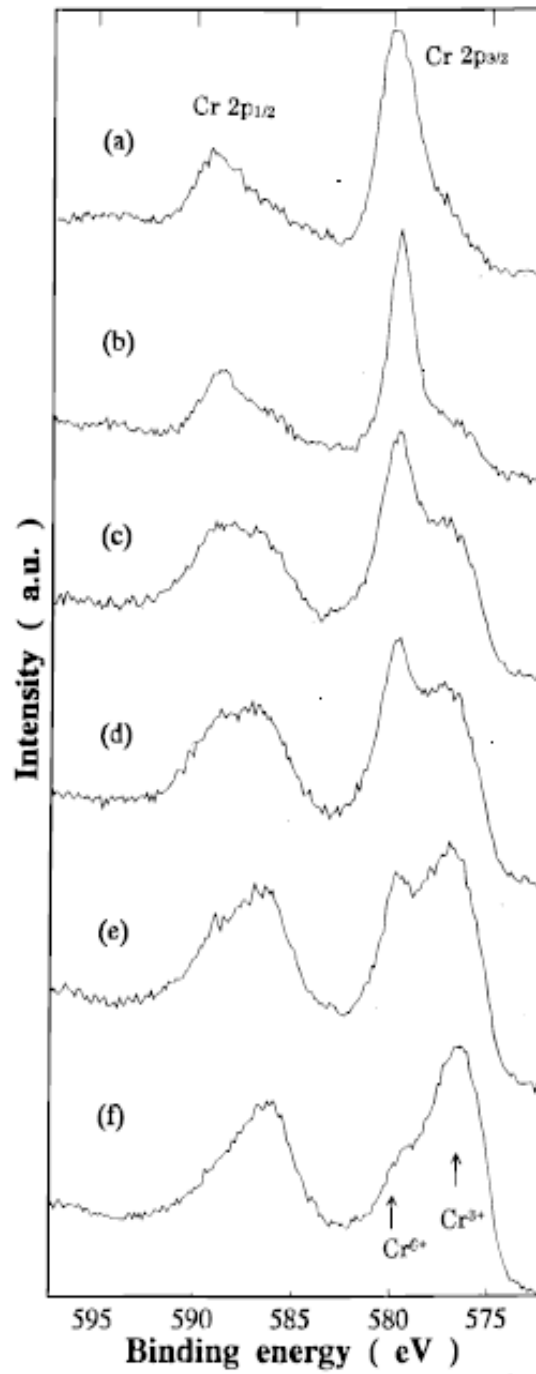
(a)

XPS ANALYSER SOURCE LABEL	Ti A:\D28005\TI.DTS CAE = 20eV STEP = 100 meV SCANS = 60 TIME = 20m 6.00s Al K-alpha Standard Ti	AM 09-29-2006
------------------------------------	---	---------------



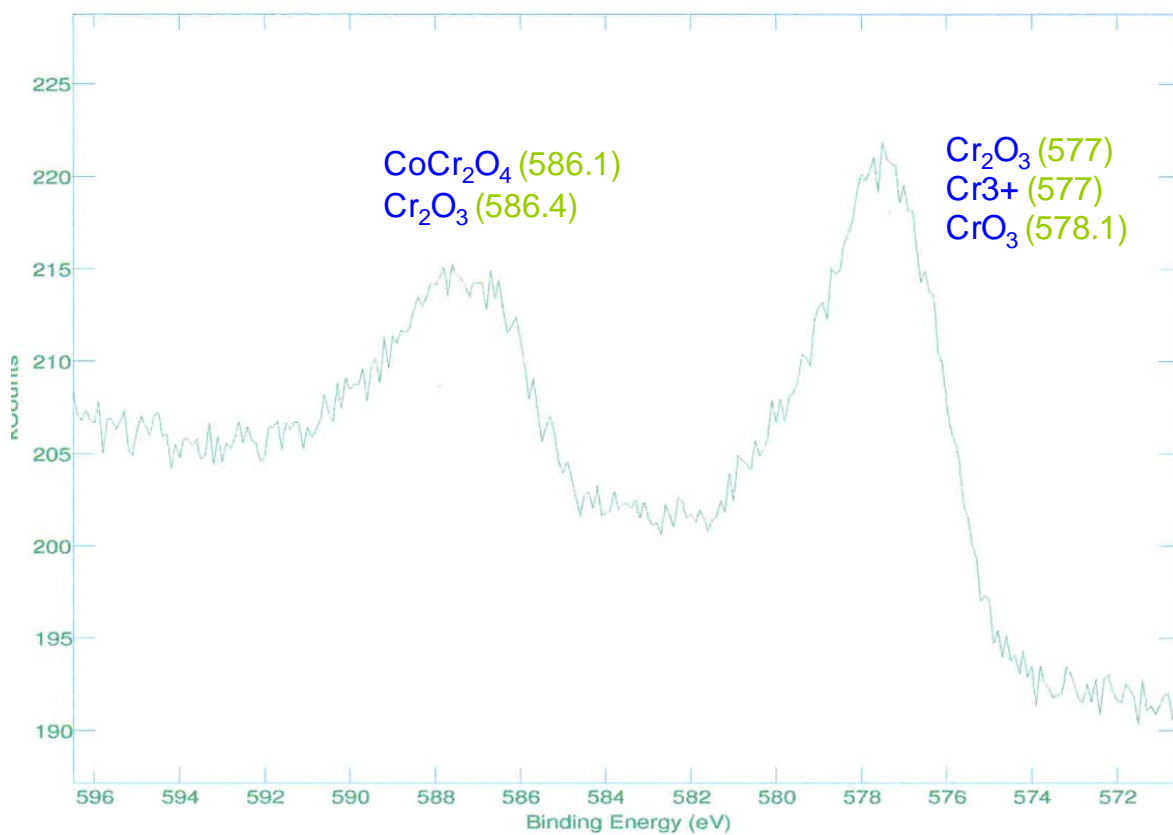
(b)

Fig. 3-11 (a), (c) XPS analysis from Handbook of X-ray Photoelectron Spectroscopy, Perkin-Elmer, Eden Prairie, MN, 1979 (b) in using 20Co/30Ti/100Al in Exp.B , (d)20Co/30Cr/100Al in Exp.B [48-49]



(c)

Fig. 3-11 (a), (c) XPS analysis from Handbook of X-ray Photoelectron Spectroscopy, Perkin-Elmer, Eden Prairie, MN, 1979 (b) in using 20Co/30Ti/100Al in Exp.B, (d)20Co/30Cr/100Al in Exp.B [48-49]



(d)

Fig. 3-11 (a), (c) XPS analysis from Handbook of X-ray Photoelectron Spectroscopy, Perkin-Elmer, Eden Prairie, MN, 1979 (b) in using 20Co/30Ti/100Al in Exp.B , (d)20Co/30Cr/100Al in Exp.B [48-49]

Both in Fig.3-11 (b) and (d), interlayer metal carbide were observed ,either in XRD analysis (Fig.3-12),in explanation of reasons Ti interlayer can be added to 150 A , still actively to CNTs growth owing to Ti metal can be transferred to TiO₂. Table.3-5(a),(b) showed the data about Heat of formation carbide, which mean the formation carbide lowered the bottom of catalyst carbon solubility, as shown in Fig.3-13 (a-c)

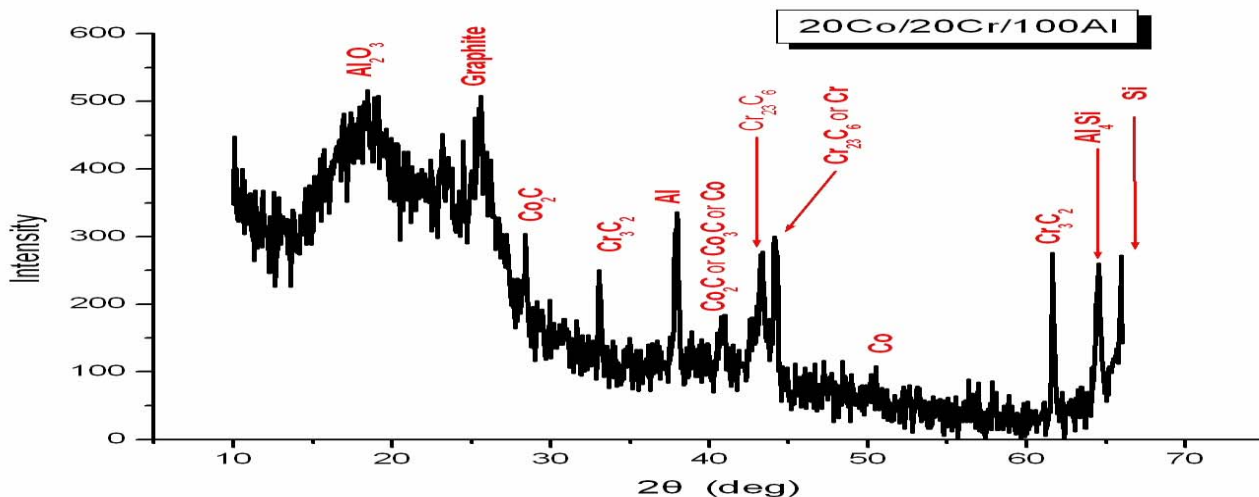
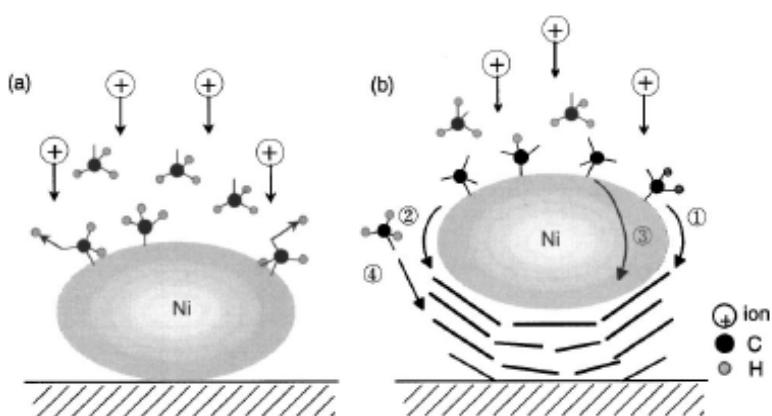


Fig. 3-12 XRD analysis for CNTs using 20Co/20Cr/100Al in the Exp. A

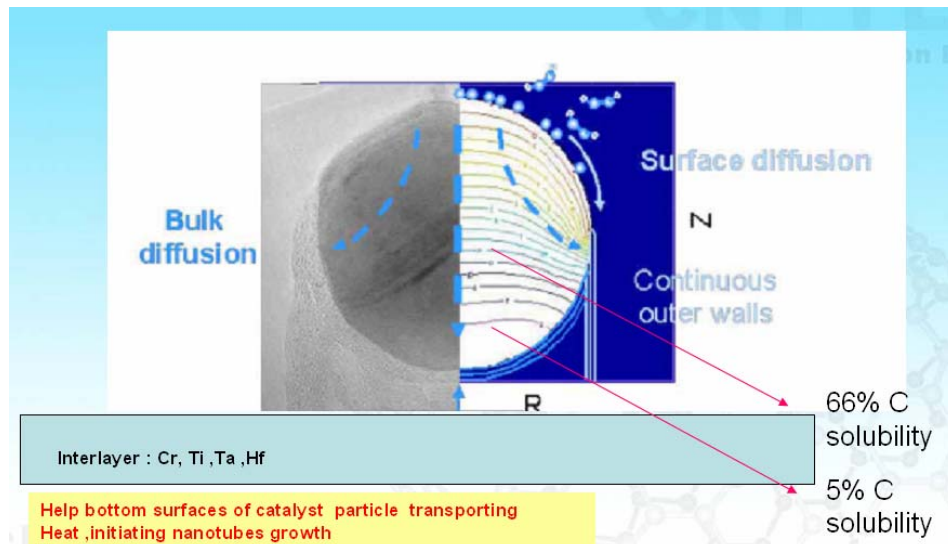
Heat of interlayer formation	
$\Delta H > 0$	Ti, Ta, Cr, Hf
$\Delta H \approx 0$	W, Mo
$\Delta H < 0$	Pt, Pd

(a)



(b)

Fig. 3-13 (a) Heat of interlayer formation carbides, (b) CNTs tip growth model, (c) interlayer below the catalyst diagram.



(c)

Fig. 3-13 (a) Heat of interlayer formation carbides ,(b)CNTs tip growth model, (c) interlayer below the catalyst diagram.

Table 3-5 (a) Heat of Formation Carbides

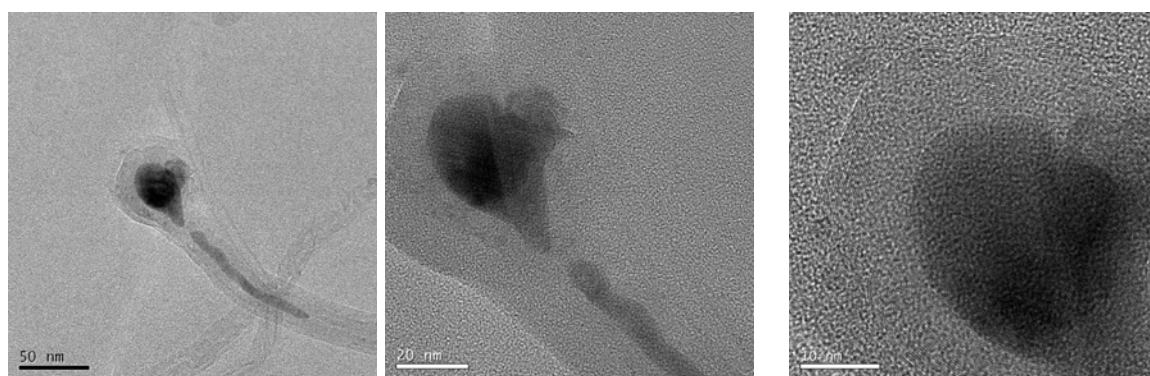
Heat of formation, ΔH of transition metal carbides, at room temp., from the metals and graphite in standard states, in electron volts per carbon atom.

Carbide	Sub lattice	$\Delta H(\text{ev})$
TiC	FCC	1.91
CrC	FCC	-0.01
C_{13}C_2	Compl.	0.442
Cr_7C_3	Compl.	0.555
Cr_{23}C_6	Compl.	0.567
FeC	FCC	-0.43
Fe_3C	Compl.	-0.22
CoC	FCC	-0.53
Co_3C	Compl.	-0.20
NiC	FCC	-0.64
Ni_3C	Compl.	-0.3
PdC	FCC	-0.66
PtC	FCC	-0.64

Table 3-5 (b) Heat of Formation Carbides

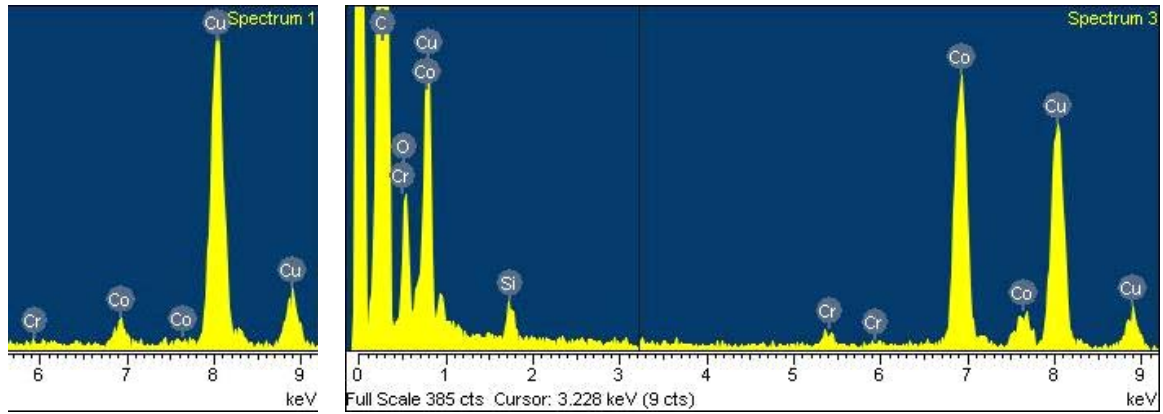
Carbide	Sub lattice	$\Delta H(\text{ev})$
TaC	FCC.	1.48
Ta ₂ C	FCC	2.16
HfC	FCC	2.17
MoC	simple	0.13
Mo ₂ C	hex	0.48
WC	simple	0.42
W ₂ C	hex	0.54

The outer graphite layer of CNT from TEM image (Fig.3-14 (a), Fig.3-15 (a)) was multi-wall structure and catalyst particle stuffed the middle of CNT. In addition, in the EDS analysis for the catalyst particle (Fig.3-14(c), Fig.3-15(d)), only Co element existed in the catalyst particle, which means that only Co took part in the CNT growth except Al and Cr. The role of Co is a catalyst for CNT growth, but Cr and Al play the supporting role for CNT growth.



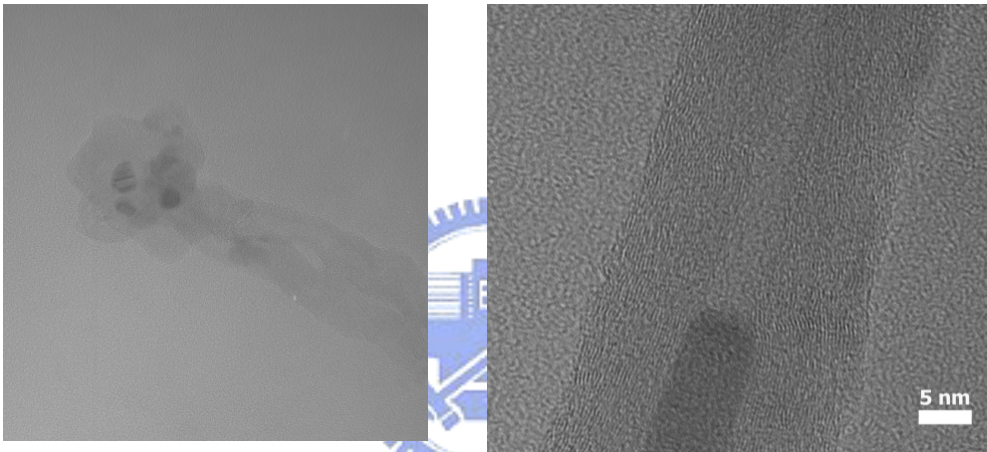
(a)

Fig. 3-14 (a) TEM analysis of CNTs growth in Exp.A using 20Co/30Ti/100Al (b) EDS analysis.



(b)

**Fig. 3-14 (a) TEM analysis of CNTs growth in Exp.A using 20Co/30Ti/100Al
(b) EDS analysis.**



(a)

**Fig. 3-15 (a) TEM analysis of CNTs growth in Exp.A using 20Co/30Cr/100Al
(b) EDS analysis.**

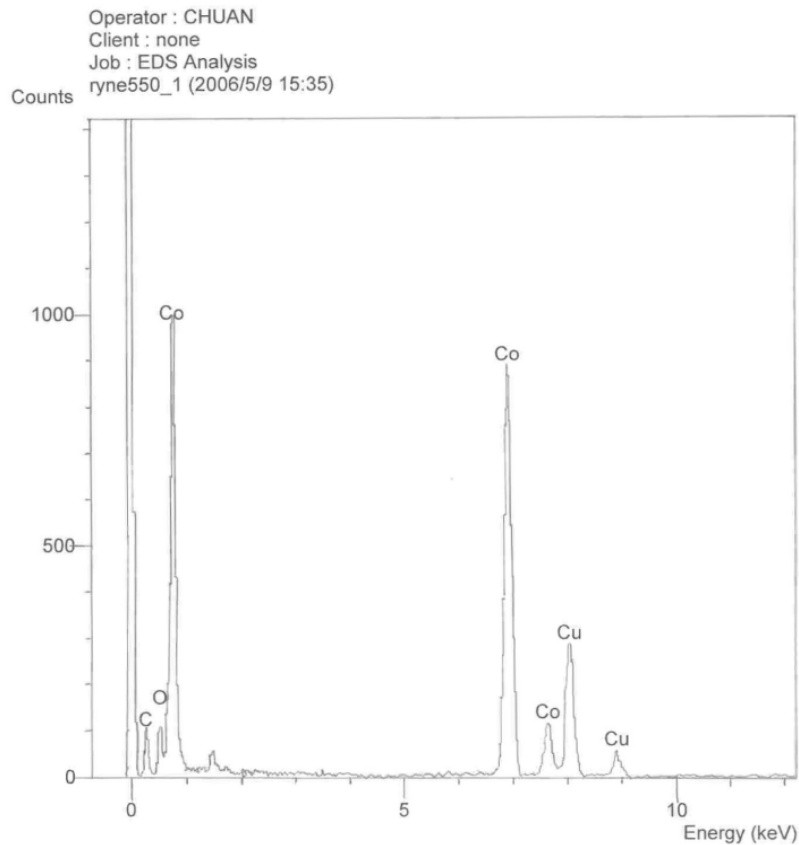
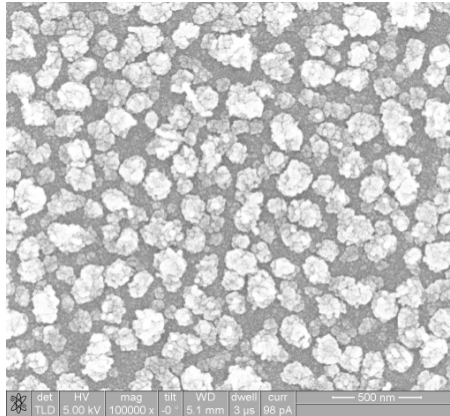


Fig. 3-15 (a) TEM analysis of CNTs growth in Exp.A using 20Co/30Cr/100Al (b) EDS analysis.

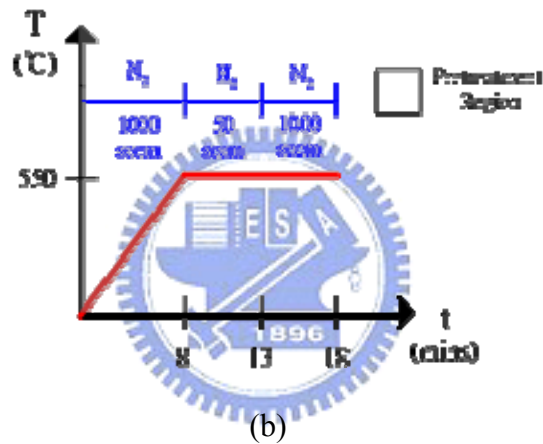
3.1.3 Effects of surface energy (Exp. C)

Particularly, it is generally believed that the formation of catalyst nanoparticles is necessary before CNT growth-pretreatment. The pretreatment method is classified by the surface energy of interlayer as show in Fig.2-5, we chose Ta, Hf, Ti, Cr to be investigated. The catalysts' nano-films were pretreated at 550°C for 5 minutes with 50 sccm H₂, and for 5 minutes with 1000sccm N₂, respectively (Fig.3-16(b)). The SEM images of pretreatment before CNT growth without interlayer are shown in (Fig.3-16(a)),



20Co/100Al

(a)

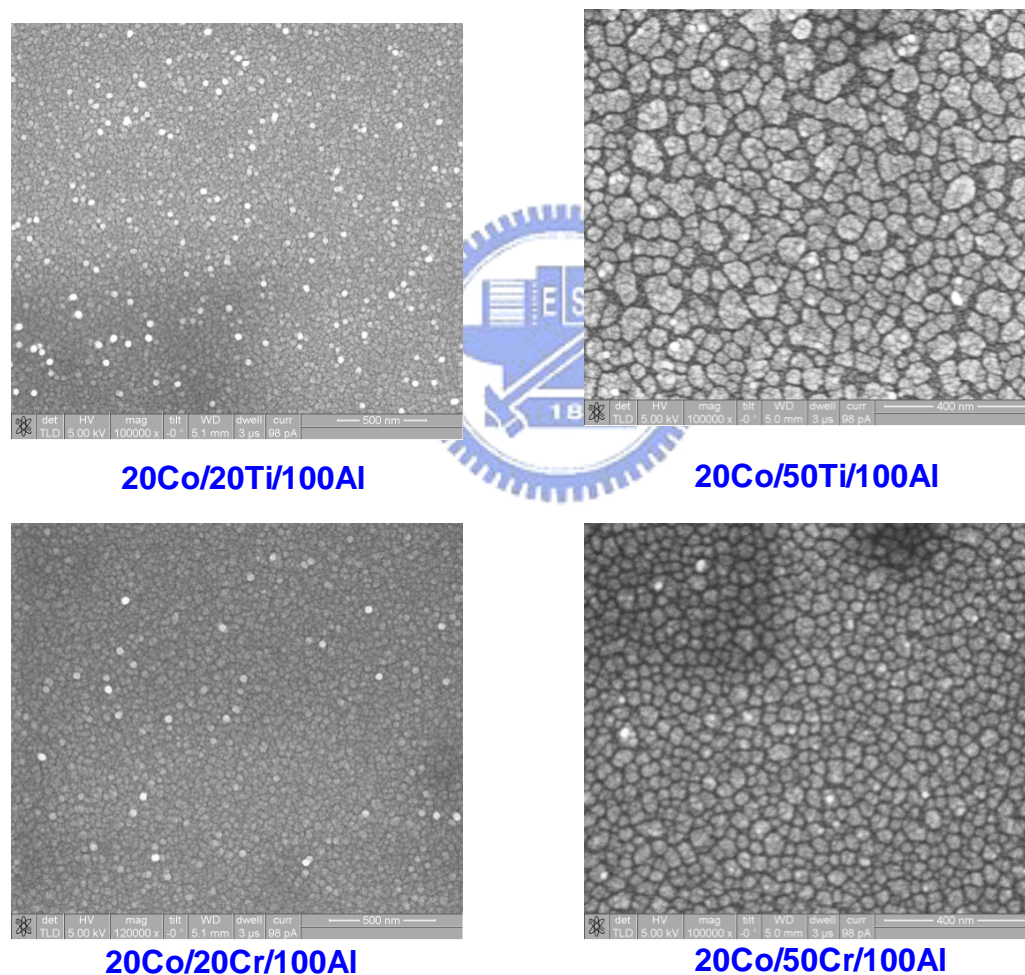


(b)

Fig. 3-16 (a) The SEM images of CNT before growth without interlayer, (b) which growth condition.

From Fig. 3-17 (a) (b), when using 20 Å thicknesses, we could significantly find out that diameter of catalyst particles is smaller while using Ti and Cr interlayer than Ta and Hf. With the interlayer thickness increased to 50 Å, catalyst particles became bigger and bigger. The effect of interlayer film on multilayer catalyst films will be discussed in this section. Via careful selection of suitable thickness of interlayer, the deposited thin catalyst layer is helpful for CNT growth at 550° C, and the results were the same as the Wang et al.[50-51]The morphology had extreme differences like

graphite respectively. The above results revealed the Cr film is dispensable in the multilayer catalyst films. From the paper researches [52-53], the Cr film could enhance adhesion between CNTs and substrate due to the formation of interface bonds. Besides, Lee et al. [54] have recently reported that the addition of Cr as co-catalyst can lower down the carbon nanotube growth temperature using Co-Ni alloy catalyst. Furthermore, in the Table 3-5, the heat formation of transition metal carbides of Co and Cr is close to -0.22ev and 0.555ev, respectively. So in the CNT growth, Cr inclines to transform into carbide type more than Co does.



(a)

Fig. 3-17 (a) The SEM images of CNT before growth using Ti , Cr interlayer, (b)Ta, Hf interlayer

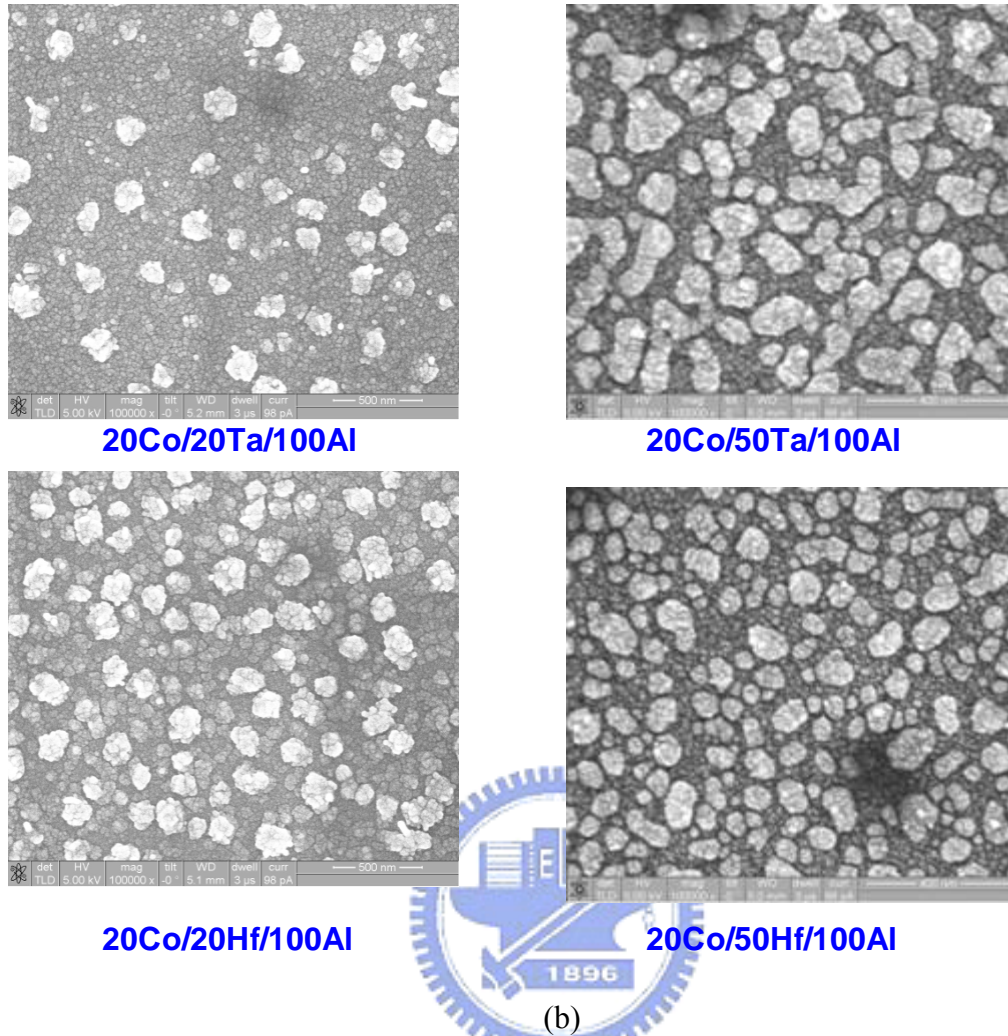



Fig. 3-17 (a) The SEM images of CNT before growth using Ti , Cr interlayer, (b)Ta, Hf interlayer

Christian P. Deck et al.[55] investigated that carbide formation inhibits nanotube growth from the pure metal, carbides could be used as potential catalysts to encourage graphite precipitation, provided the appropriately sized carbide particles and carbon diffusion was fast enough. From the proof of XRD analysis (Fig. 3-12) using 20Co/20Cr/100Al in Exp. A, we could find that Cr carbide (Cr_3C_2 and Cr_{23}C_6) existed onto the CNT bottom. To sum up, Cr could enhance adhesion between CNT and substrate and Cr carbide could disperse carbon atoms uniformly so that CNT could be grown well when Co achieved carbon saturation to precipitate carbon atoms.

The above has mentioned each function of multilayer catalyst films. The EDS analysis (Fig. 3-15(b)) revealed CNT growth was dominated by Co catalyst. Cr could enhance adhesion between CNT and substrate, and Cr carbide could disperse carbon atoms uniformly so that CNT could be grown well. Al film could transform into stable Al_2O_3 , which could prevent catalyst particles from merging together and increased the number of active sites. In the Exp. B, we investigated the effect of interlayer thickness on the same under multilayer catalyst films, and survey on heat of formation carbide was included, in addition. We listed the comparison in Table.3-6, which showed suitable surface energy and formation heat and improves CNTs growth at low temperature.

Table 3-6 Surface Energy vs. Formation Heat

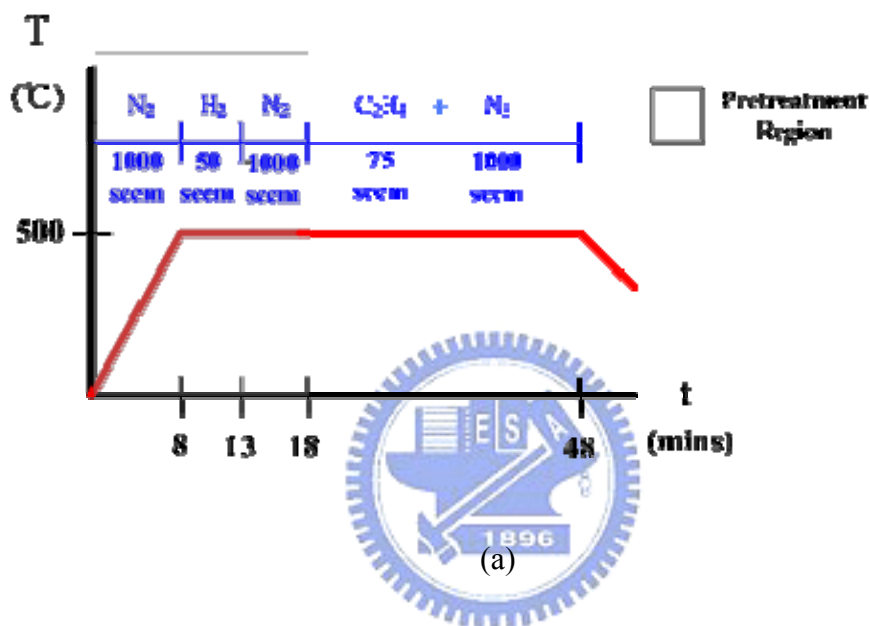


Surface Energy \ Formation Heat	>Co	≈ Co	<Co
$\Delta H > 0$	Ta	Ti, Cr	Hf
$\Delta H \approx 0$	Mo, W		Cu
$\Delta H < 0$		Pt	Pd

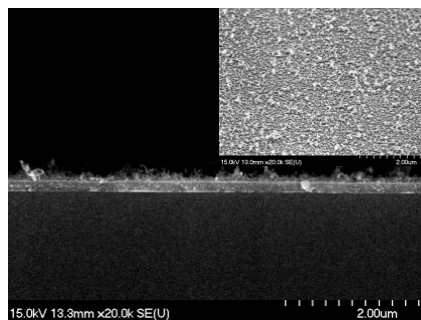
3.1.4 Effect of Growth Temperature (Exp. D)

In order to prove the effect of growth temperature on the surface diffusion of CNT growth mechanism, we synthesized CNTs at 500° C (Fig.3-18(a)) as shown in Fig2-7(d), and set up the model without interlayer referring to Fig.3-18(b). From the morphology of CNT cross-section images (Fig.3-19 (a)-(c)), the field emission

measurements were showed in the Fig. 3-20. The field emission characteristics were shown in the Table. 3.7. By Raman analysis in Fig.3-20 & 3-21, we could significantly find out the field emission properties got better and better because the Cr, Ti were deposited as interlayer. Especially, the thickness was taken 30 Å, the anode current at 6V/um was achieved to 4.16mA/cm², 3.41mA/cm² superior than others combinations.

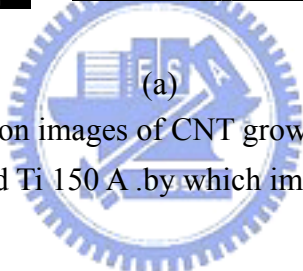
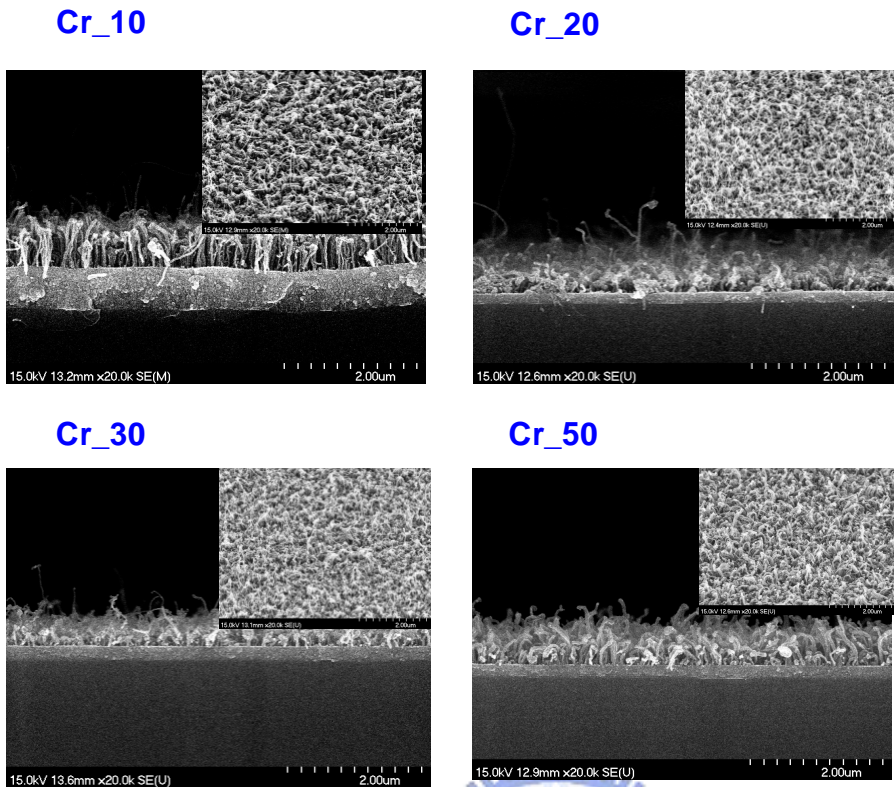


20Co/100Al

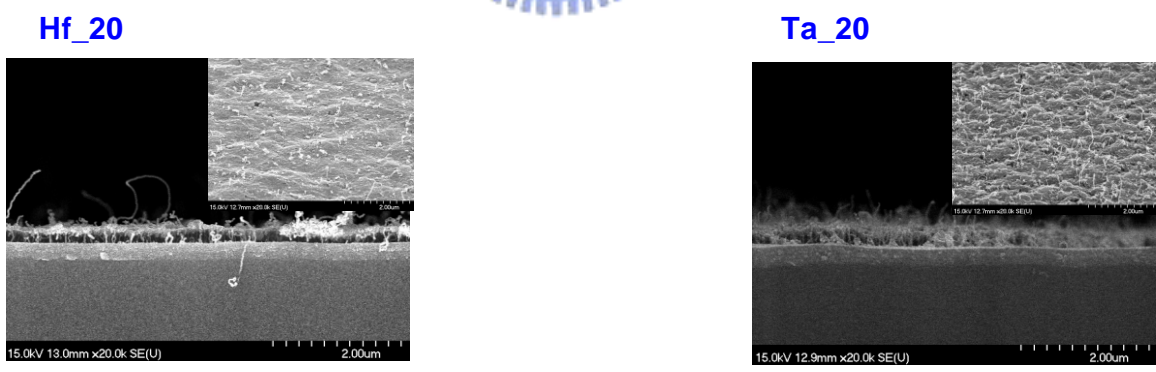


(b)

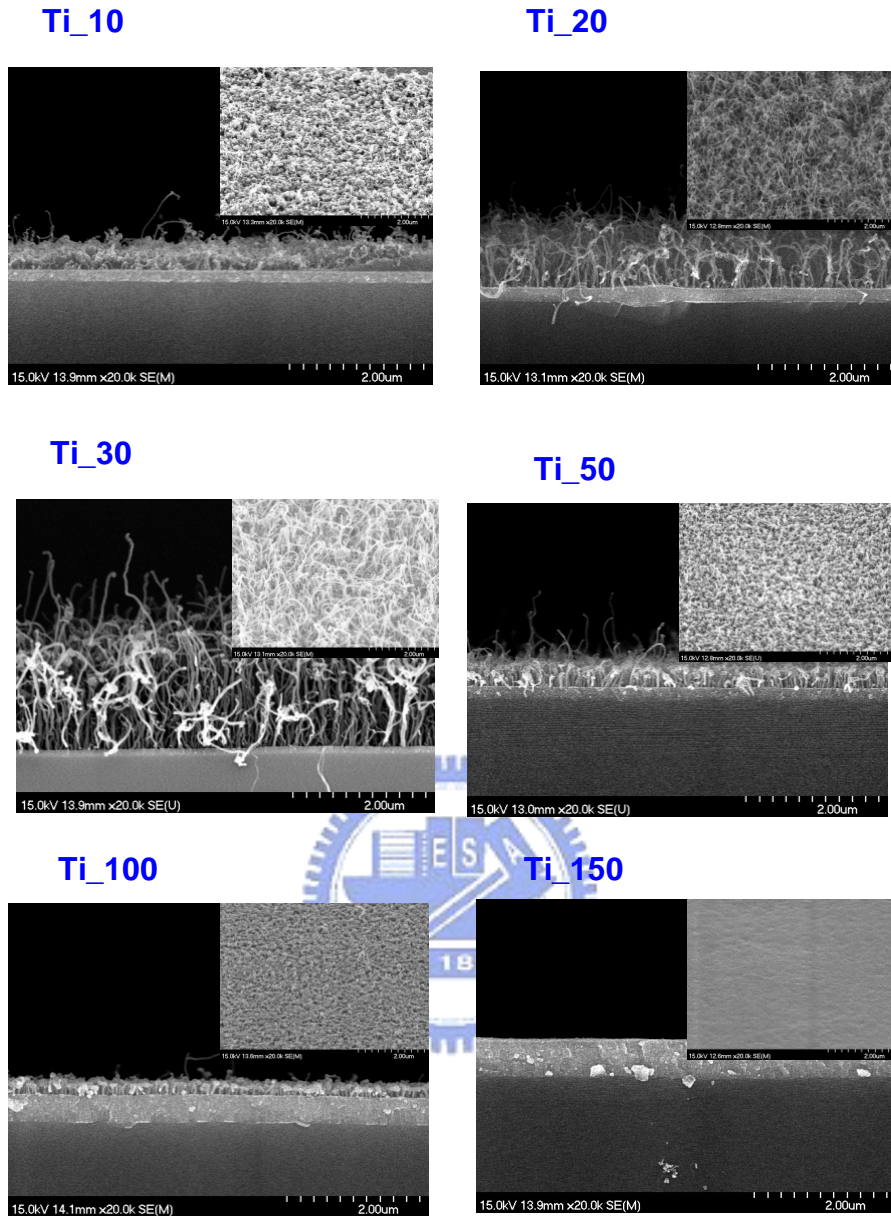
Fig. 3-18 (a) The SEM cross-section images of CNT growth without interlayer and image represents the top view image of, (b) which growth condition.



(a)
 Fig. 3-19 The SEM cross-section images of CNT growth at 500°C with interlayer of (a) Cr 100 A , (b) Ti 100 A, and Ti 150 A .by which image represents the top view .



(b)
 Fig. 3-19 The SEM cross-section images of CNT growth at 500°C with interlayer of (a) Cr 100 A , (b) Ti 100 A, and Ti 150 A .by which image represents the top view .



(c)

Fig. 3-19 The SEM cross-section images of CNT growth at 500°C with interlayer of (a) Cr 100 Å, (b) Ti 100 Å, and Ti 150 Å. by which image represents the top view.

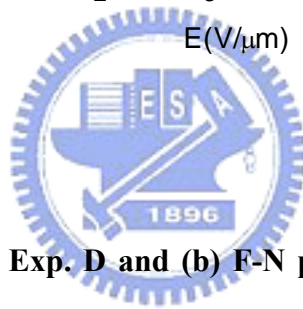
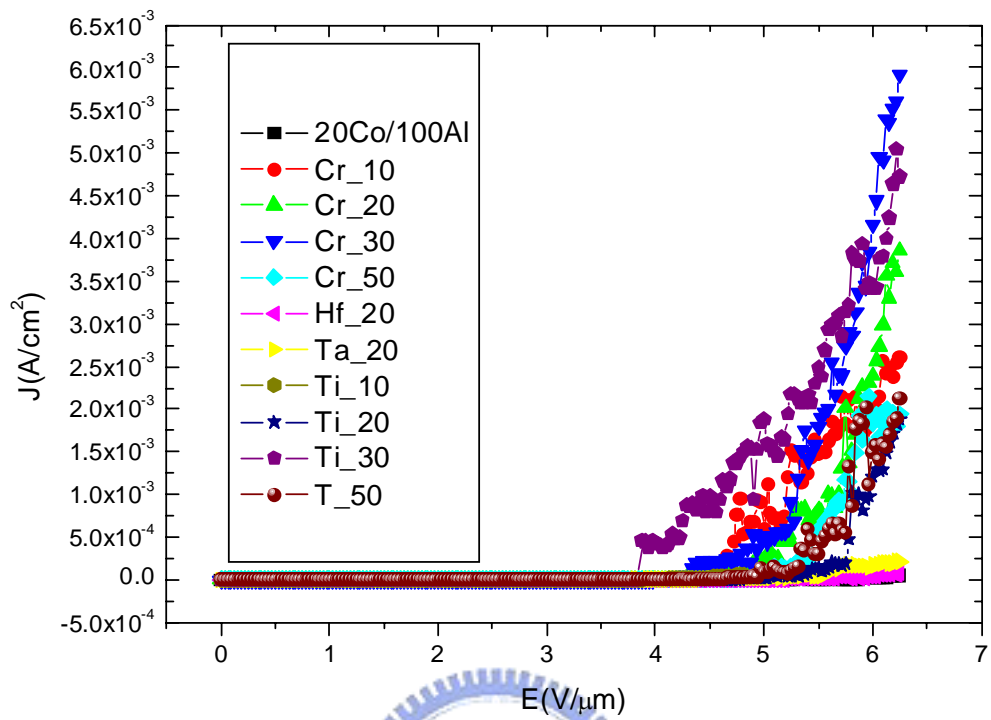
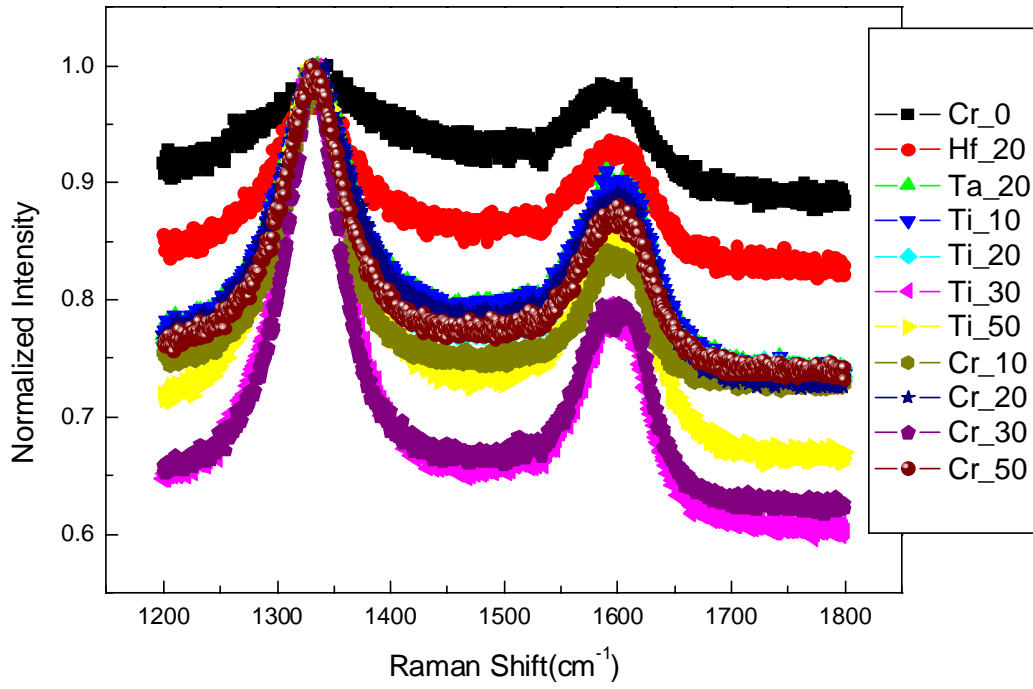
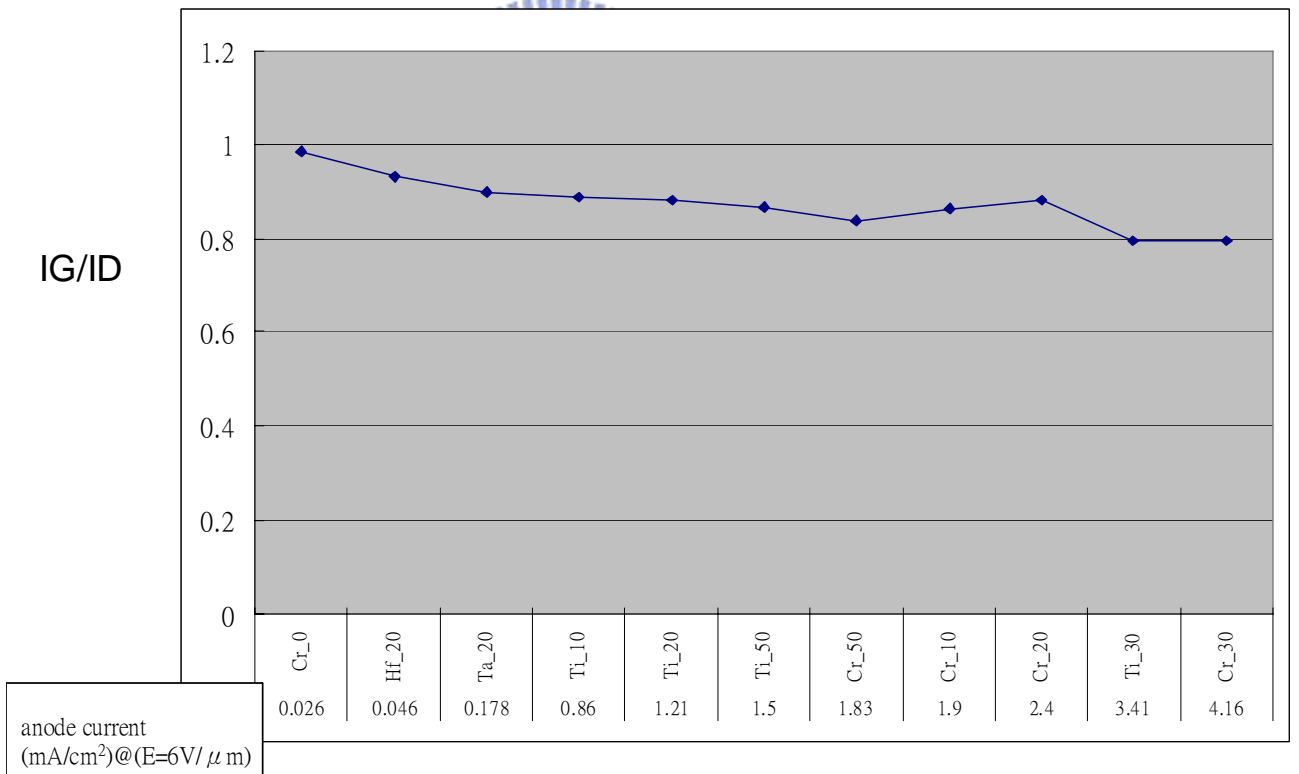


Fig. 3-20 (a) I-V plot in the Exp. D and (b) F-N plot in the Exp. D (Effect of Growth Temperature)



(a)



(b)

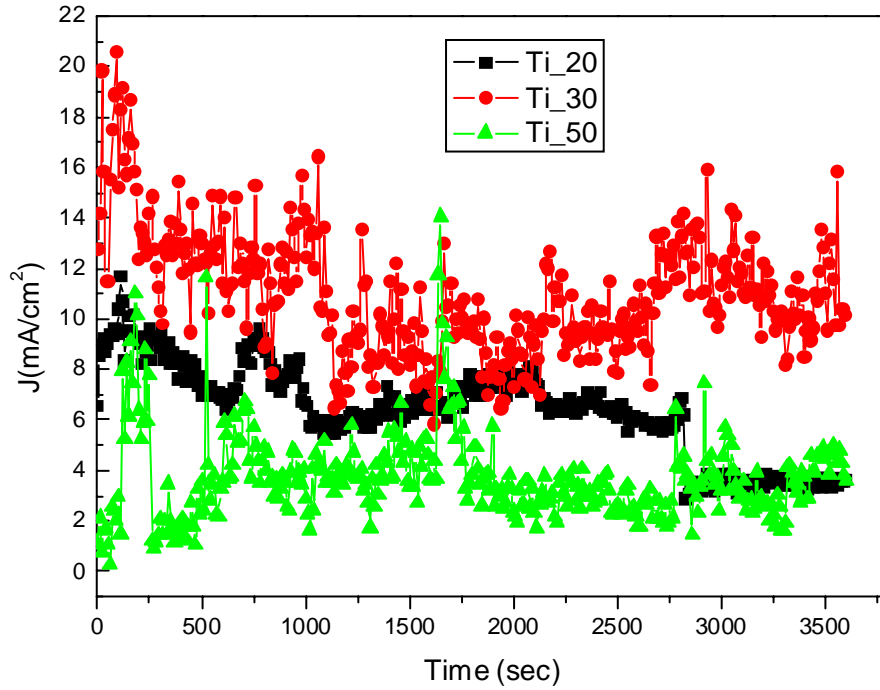
Fig. 3-21 Raman analysis in Exp. D ; (a) G peak at 1590 cm⁻¹ and D peak at 1330 cm⁻¹, (b) IG/ID ration vs. anode current density .

Table 3-7 Field emission characteristics in Exp.D (Effect of Growth Temperature)

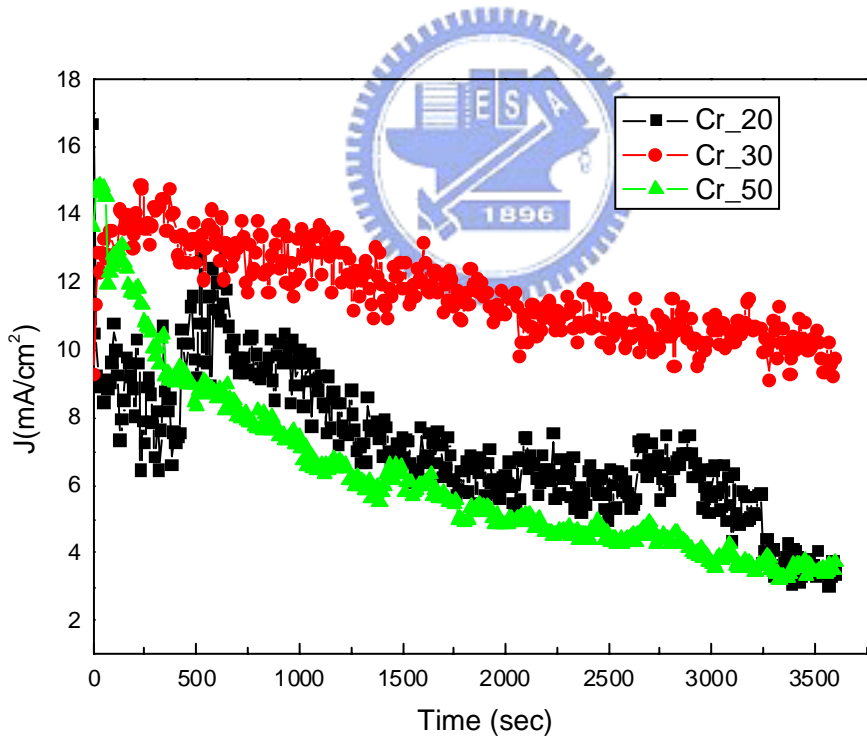
	20Co/100Al	Cr_10	Cr_20	Cr_30	Cr_50	Hf_20	Ta_20	Ti_10	Ti_20	Ti_30	Ti_50
Turn on Field (V/ μm)@ ($J=10\text{ nA}/\text{cm}^2$)	4.375	4.31	4.28	4.03	4.75	5.21	4.375	4.09	4.78	3.875	4.28
Anode Current (mA/cm^2)@ ($E=6\text{ V}/\mu\text{m}$)	1.95	1.9	2.4	4.16	1.83	0.046	0.178	0.86	1.21	3.41	1.5

3.1.5 Stress test (Exp. E)

Both samples were grown in 550°C and 500°C by each, The electric characteristics were measured by Keithley 237 in a 10^{-6} torr chamber for stress test by 1 hr, and anode applied 1000V, the spacer between anode to cathode was 160 μm and the simple dimension was 1mm x 1mm. We surveyed the Ti 20 A, Ti 30 A, Ti 50 A, Cr 20 A, Cr 30 A, and Cr 50 A. The results are shown in Fig.3-22 and Fig.3-23, summarized in Table.3-8 and Table.3-9. From Table.3-8, when growth temperature was at 550°C, Ti 30 A demonstrated the superior field characteristics no matter in what variation coefficient (22.21%) or anode current density ($10.6\text{ mA}/\text{cm}^2$), the other combination Cr 30 A, also had nice reliability whose variation coefficient (11.71%), anode current density ($10.4\text{ mA}/\text{cm}^2$) obviously differ from other thicknesses. Then, we extended the test time to 10 hours, the results are shown in Fig.3-24 and Table.3-10. We also applied an ITO glass with phosphor coating on it as the anode observed the luminescent image (Fig. 3-25), which showed excellent field emission and uniform light sight.

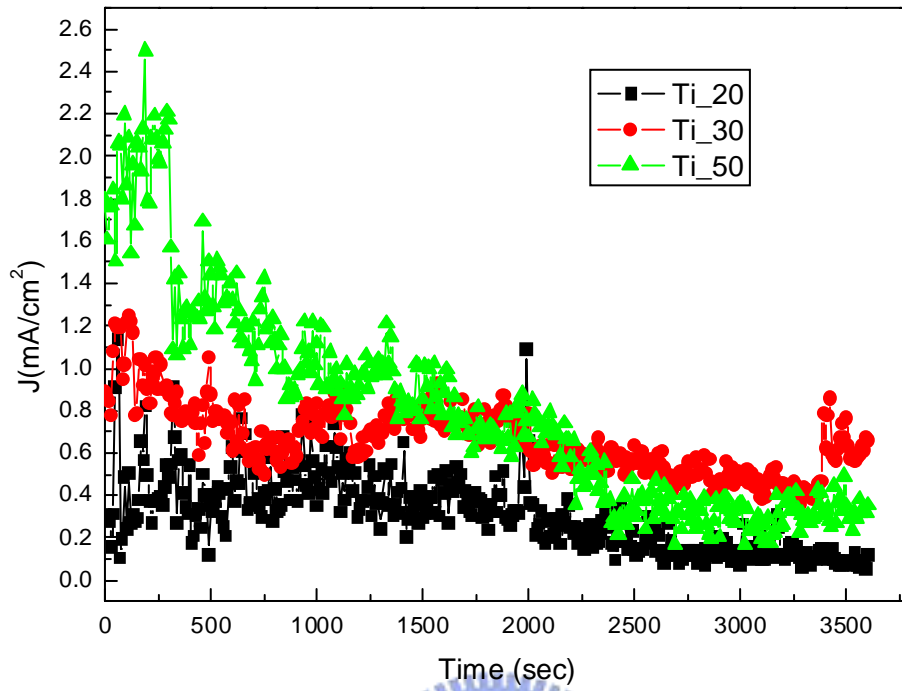


(a)

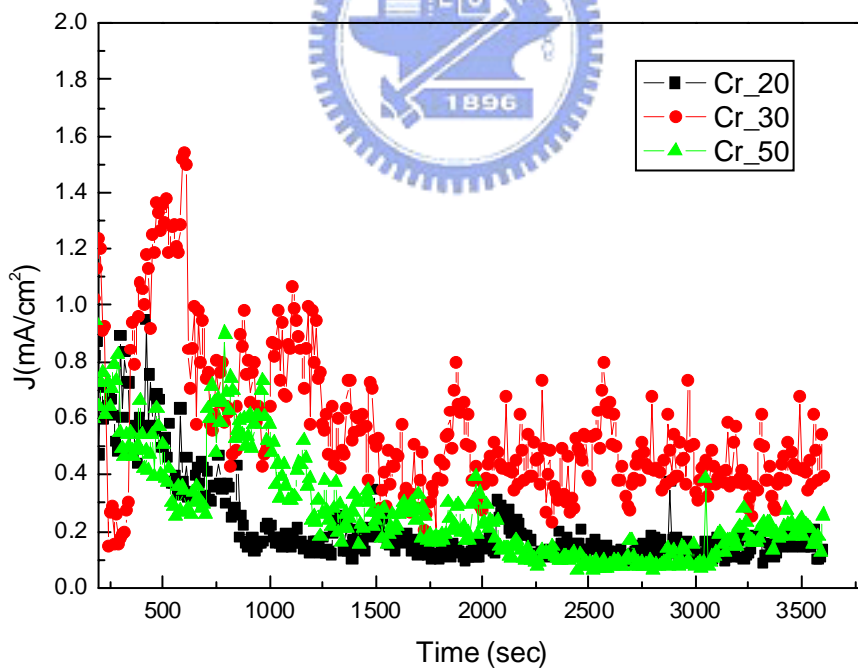


(b)

Fig. 3-22 stress test in Exp. E at 550°C; (a) Ti interlayer : 20 A, 30 A, 50 A. (b) Cr interlayer : 20 A, 30 A, 50 A.



(a)



(b)

Fig. 3-23 stress test in Exp. E at 500°C; (a) Ti interlayer : 20 A, 30 A, 50 A. (b) Cr interlayer : 20 A, 30 A, 50 A.

Table 3-8 Stress test at 550°C in Exp. E (a) Ti 20 A, Ti 30 A, and Ti 50 A (b) Cr 20 A, Cr 30 A, and Cr 50 A

(a)

	Ti_20	Ti_30	Ti_50
STD	1.83	2.45	1.75
AV(mA/cm ²)	6.37	11.01	3.70
C.V	28.68%	22.21%	47.41%
Final(mA/cm ²)	3.5	10.6	3.4

(b)

	Cr_20	Cr_30	Cr_50
STD	2.08	1.28	2.57
AV(mA/cm ²)	7.14	11.71	6.19
C.V	29.09%	10.93%	41.50%
Final(mA/cm ²)	4.4	10.4	3.58

Table 3-9 Stress test at 500°C in Exp. E (a) Ti 20 A, Ti 30 A, and Ti 50 A (b) Cr 20 A, Cr 30 A, and Cr 50 A

(a)

	Ti_20	Ti_30	Ti_50
STD	0.18	0.17	0.50
AV(mA/cm ²)	0.31	0.67	0.81
C.V	58.55%	24.85%	61.88%
Final(mA/cm ²)	0.1	0.6	0.33

(b)

	Cr_20	Cr_30	Cr_50
STD	0.21	0.48	0.62
AV(mA/cm ²)	0.25	0.64	0.36
C.V	83.07%	75.31%	169.18%
Final(mA/cm ²)	0.15	0.42	0.2

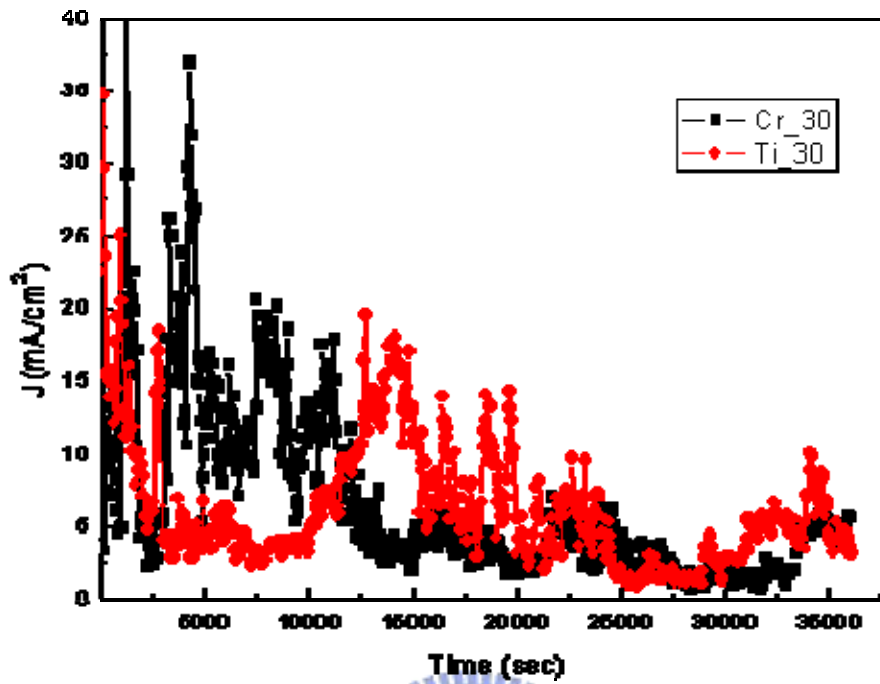


Fig. 3-24 Stress test in 10 Hours with Ti 30 A and Cr 30 A

Table 3-10 Stress test in 10 Hours with Ti 30 A and Cr 30 A

	Cr_30	10 Hours	Ti_30
STD	6.30		5.87
AV(mA/cm ²)	5.91		3.96
C.V	93.81%		67.39%
Final(mA/cm ²)	3.02		4.35

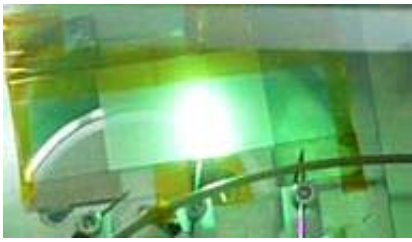

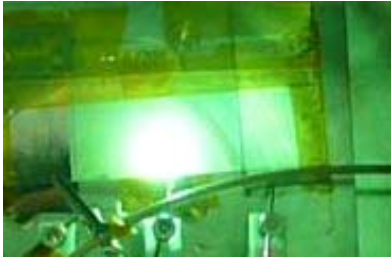

	550 °C	500 °C
Ti_30		
Cr_30		

Fig. 3-25 Luminescent image in Exp. E .(Stress test)

3.2 Gated Triode Structure (Exp. F)

The stress test in Exp.E was taken into consideration, so the optimum thickness was chosen to be 30 Å. The promising multilayer catalyst films (20Å Co/ 30Å Cr/ 100Å Al) and (20Å Co/ 30Å Ti/ 100Å Al) had been investigated (i.e. the morphology and field emission characteristics of CNTs). Further, we fabricated the low temperature triode structure in order to realize low voltage driving, high resolution and full gray-scale imaging using multilayer catalyst films. In the past years, many researches have investigated the triode structure [56] (poly Si/SiO₂/cathode), but their fabrication temperature was higher than 550° C whose temperature is the melting point of sodalime glass substrate. Although they could achieve the excellent field emission properties, their methods had no values on the display applications. In our current study, the Cr gate/SiO₂/Cr cathode triode structure was realized and its fabrication temperature was below 350°C. We had to control the CNT length to prevent CNTs across the Cr gate and cathode so that the Cr gate had to be

side-etching for 2-3 μm by HDP-RIE dry etching. As the Fig.2-8(c) shows, the insulated gate structure field emission triodes avoid the short circuit problem between cathode and gate, so the morphology of CNTs (Fig.3-26(a) and (b)) in the triode was extremely different from ones in the diode using the same growth recipes (Exp. A and Exp. D). Therefore the growth recipe had to be improved in order to enhance the ability of CNT growth by adding the growth time. In the Fig. 3-26, the length of CNTs was short and it seemed to have cluster CNTs. Those results were similar to Kyung Moon Lee et al.'s investigations [57]. In the Fig.3-27 and Fig.3-28, the morphology of CNTs were better. The field emission measurements and characteristics were shown in the Table 3-11, respectively. The spacer was 550 μm between cathode and anode. The Keithley 237, 238 and 238 were applied on the ITO anode (1000v), Cr gate (-30-80v), and Cr cathode (ground). The Table.3-11(a) and Table.3-11(b) showed detail the field emission measurements and characteristics except that growth time was 60 min, then the shortcut problem happened because CNTs length was too long (in Fig.3-28 (a) and Fig.3-29(b)). In 30 min growth time, the Ti 30 A showed anode current (6.24 mA/cm^2) gate current (4 mA/cm^2) at 80 V/ μm and field emission efficiency was 39.04%. Cr 30 A showed anode current (4 mA/cm^2) gate current (19 mA/cm^2) at 80 V/ μm and field emission efficiency was 17.39%. In order to improve the emission currents, growth time was added to 45 min, the Ti 30 A showed anode current (12.38 mA/cm^2) gate current (81.6 mA/cm^2) at 80 V/ μm and field emission efficiency was lowered to 13.17%. Cr 30 A showed anode current (21.6 mA/cm^2) gate current (196.4 mA/cm^2) at 80 V/ μm and field emission efficiency was changed to 9.91%. Then, we also research growth temperature at the 500°C . The Fig.3-29 showed the bad morphology of CNTs growth on 30 min growth time. So far we made great efforts on the low temperature triode structure to added time to 45 min (Fig.3-30), and 60 min (Fig.3-31). Table.3-12 revealed 45 min growth time at 500°C

whose field emission efficiency was better than others. Ti 30 A showed anode current (1.8 mA/cm^2) gate current (29.1 mA/cm^2) at 80 V/um and field emission efficiency was 5.83%.and Cr 30 A showed anode current (1.91 mA/cm^2) gate current (21.8 mA/cm^2) at 80 V/um and field emission efficiency was 8.06%.Fig.3-32 demonstrated Luminescent image at 550°C for 45 min growth time, whose dimension was described in Fig.3-33.

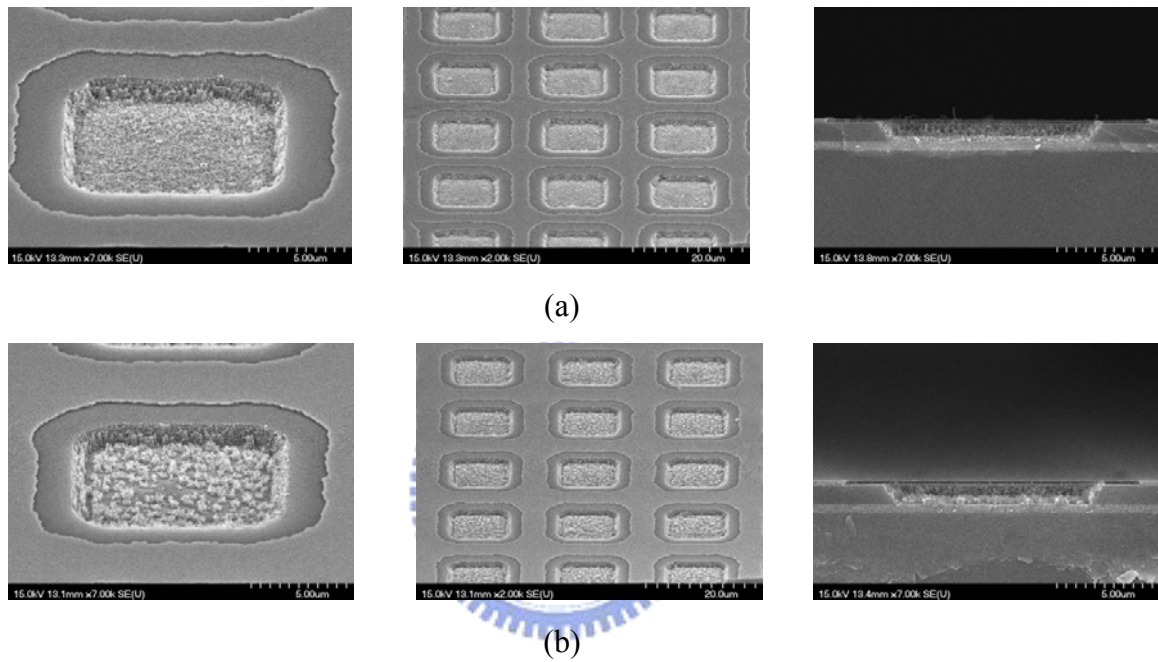
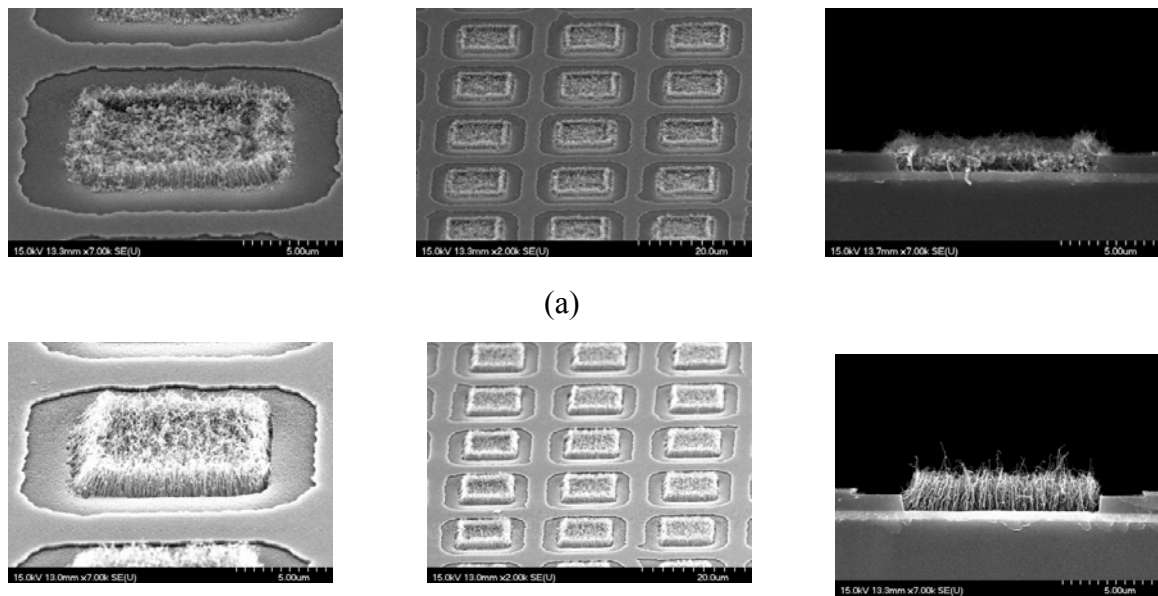
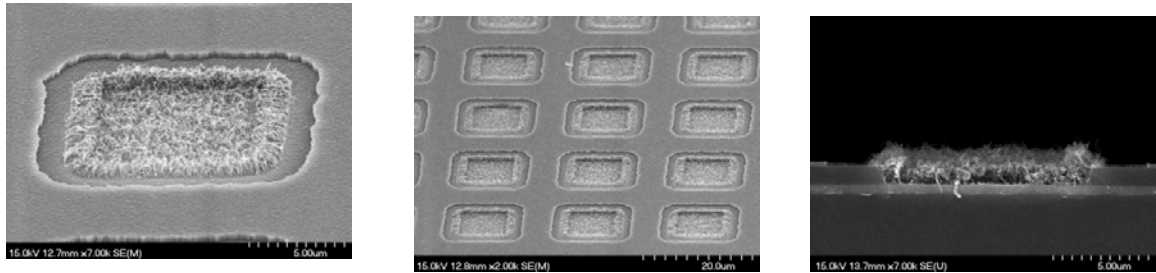


Fig. 3-26 The SEM top views and cross-section images of CNT grow with Triode structure using (a) Cr 30 A (b) Ti 30 A , at 550°C for 30 min.

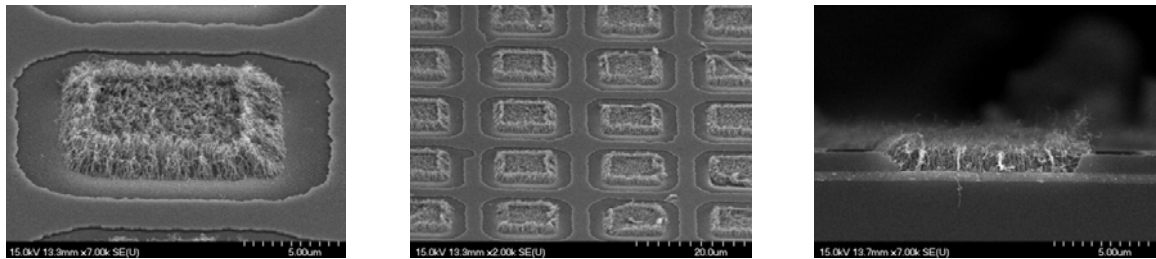


(b)

Fig. 3-27 The SEM top views and cross-section images of CNT grow with Triode structure using (a) Cr 30 A (b) and Ti 30 A , at 550 °C for 45 min.

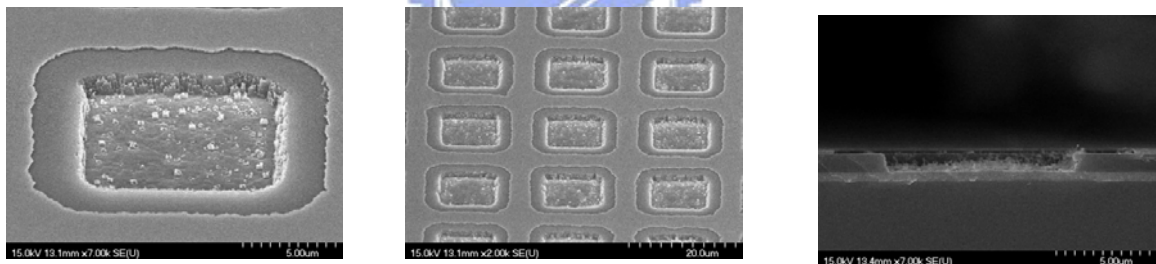


(a)

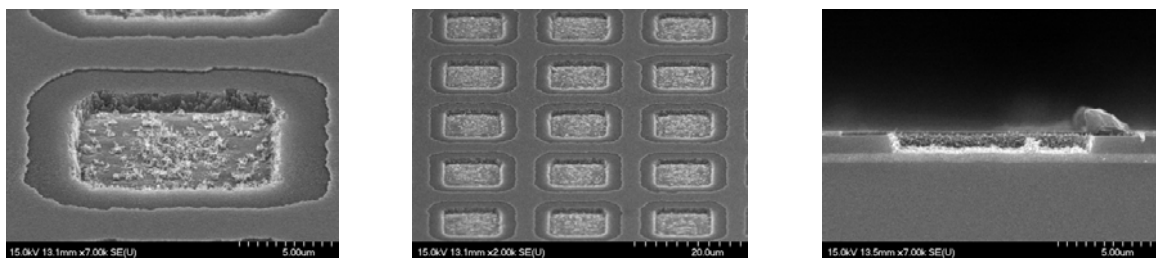


(b)

Fig. 3-28 The SEM top views and cross-section images of CNT grow with Triode structure using (a) Cr 30 A (b) and Ti 30 A , at 550 °C for 60 min.

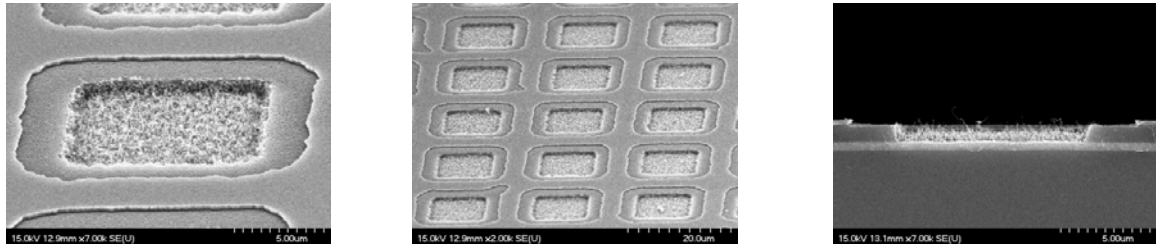


(a)

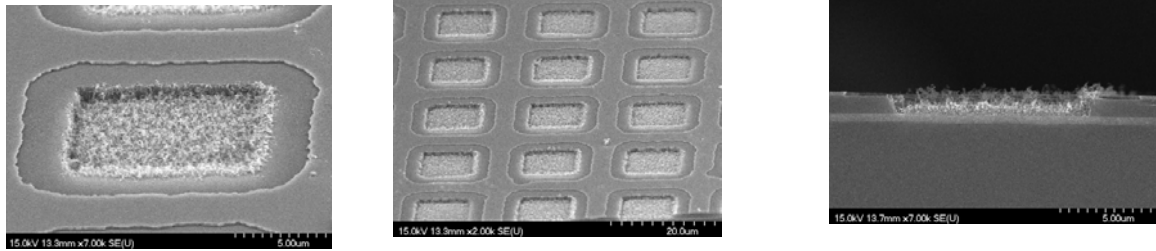


(b)

Fig. 3-29 The SEM top views and cross-section images of CNT grow with Triode structure using (a) Cr 30 A (b) Ti 30 A , at 500 °C for 30 min.

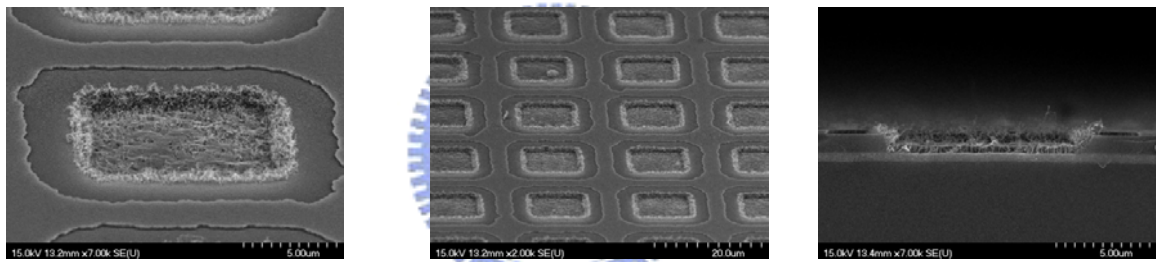


(a)

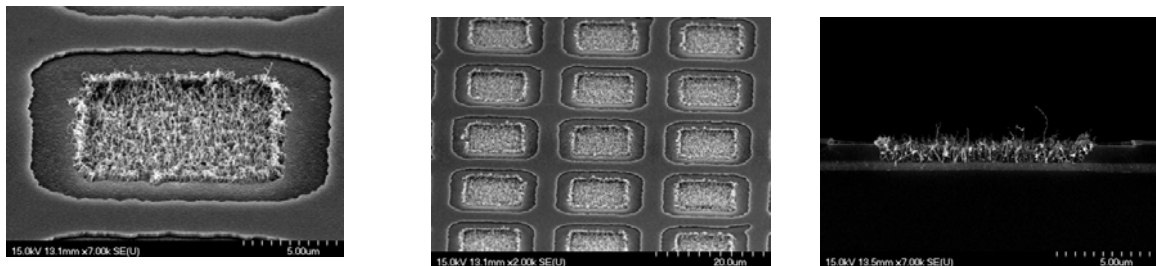


(b)

Fig. 3-30 The SEM top views and cross-section images of CNT grow with Triode structure using (a) Cr 30 A (b) Ti 30 A , at 500°C for 45 min.



(a)



(b)

Fig. 3-31 The SEM top views and cross-section images of CNT grow with Triode structure using (a) Cr 30 A (b) Ti 30 A , at 500°C for 60 min.



Ti_30



Cr_30

Fig. 3-32 Luminescent image in Exp. E at 550°C for 45 min growth time.

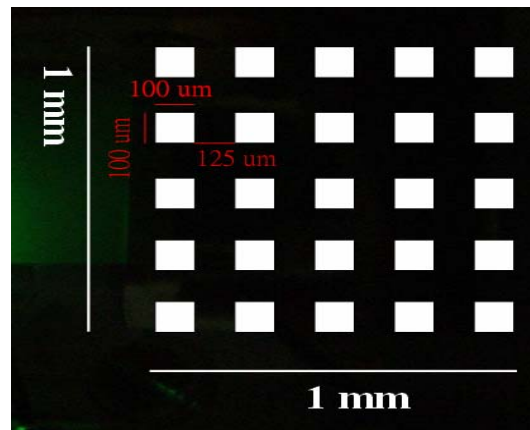


Fig. 3-33 The pattern with 25 dies, which dimension was $100 \mu m^2$ in 1mm x 1mm.

Table 3-11 Stress test at 550°C in Exp. F. by each in 30 min , 45 min, and 60 min

(a) Ti 30 A (b) Cr 30 A

(a)

	30 min	45 min	60 min
IG (mA/cm ²)	6.24	81.6	
IA (mA/cm ²)	4	12.38	
Field efficiency	39.06%	13.17%	

(b)

	30 min	45 min	60 min
IG (mA/cm ²)	19	196.4	
IA (mA/cm ²)	4	21.6	
Field efficiency	17.39%	9.91%	

Table 3-12 Stress test at 500°C in Exp. F. by each in 30 min , 45 min, and 60 min

(a) Ti 30 A(b) Cr 30 A

(a)

Ti_30	30 min	45 min	60 min
IG (mA/cm ²)	5.76	29.1	185.6
IA (mA/cm ²)	0.1	1.8	1.6
Field efficiency	1.71%	5.83%	0.85%

(b)

Cr_30	30 min	45 min	60 min
IG(mA/cm ²)	6.72	21.8	102.8
IA(mA/cm ²)	0.1	1.91	3.39
Field efficiency	1.47%	8.06%	3.19%

In sum, improvement of gate controlled anode current CNT-triodes was proposed and characterized emission properties were very superior and had high field emission efficiency. In future low temperature triode structure on glass substrate will be realized in our FED group.

3.3 CNT-FED on Glass Substrate for Diode Structure (Exp. G)

Since sodalime glass is commonly used as a low-cost substrate for the display panel, it inclines to grow CNTs directly on the sodalime glass substrate. However, sodalime glass is known to deform and degrade above 570 °C so that we proceeded our experiments at 550°C and 500°C to avoid the melt of the glass. The fabrication procedure was shown in the Fig. 2-9. However Mo and Cr [58] are usually applied as the cathode electrode in CNT-FED on glass substrate, we chose Cr as the cathode electrode material in our experiment and used 20A Co/30A Cr/100A Al and 20A

Co/30A Ti /100A Al as the catalysts to grow CNTs, and growth condition is described in Fig.3-34

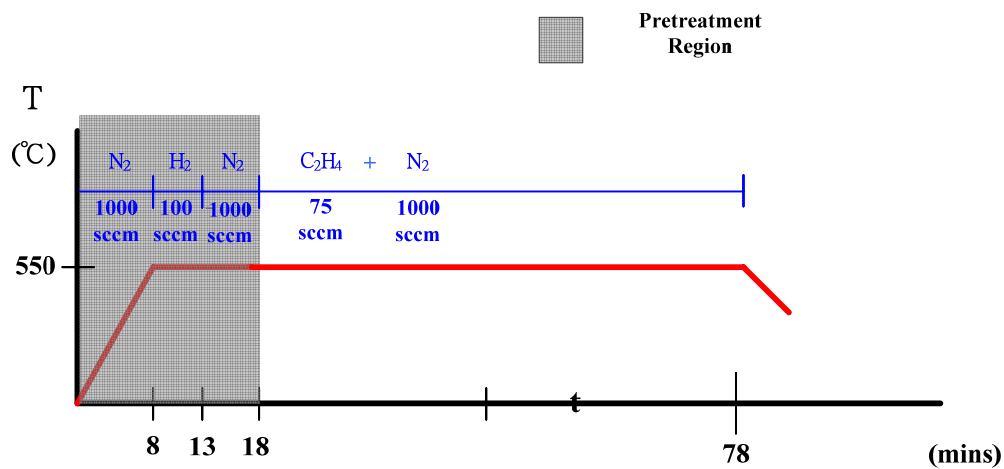


Fig. 3-34 Growth condition in Exp.G [CNT-FED on Glass Substrate for Diode Structure]

In Fig.3-35, SEM image of CNTs grown with 20A Co/30A Cr/100A Al and 20A Co/30A Ti/100A Al as the catalysts on glass substrate by thermal CVD for 60 min at 550°C and 500°C. From the morphology of CNTs growth at 500°C, CNTs were curly and sparse. We holed on stress test by measuring by Keithley 237 in a 10^{-6} torr chamber for stress test by 1 hr, and anode applied 1000V, the spacer between anode to cathode was 160 μ m and the simple dimension was 1mm x 1mm, the results was shown in Fig.3-36.and the filed emission characteristics were listed in Table.3-13. At 550°C Ti 30 A showed excellent filed emission current density with 24.9 mA/cm², and Cr 30 A was 20.5 mA/cm², respectively. However, it is gratified that we have fabricated CNT-FED on glass substrate by thermal CVD successfully, and Fig.3-37 showed luminescent image by this experiment and we believe that the novel catalysts investigated in this thesis will improve the synthesis of CNT on flat-panel FED by thermal CVD.

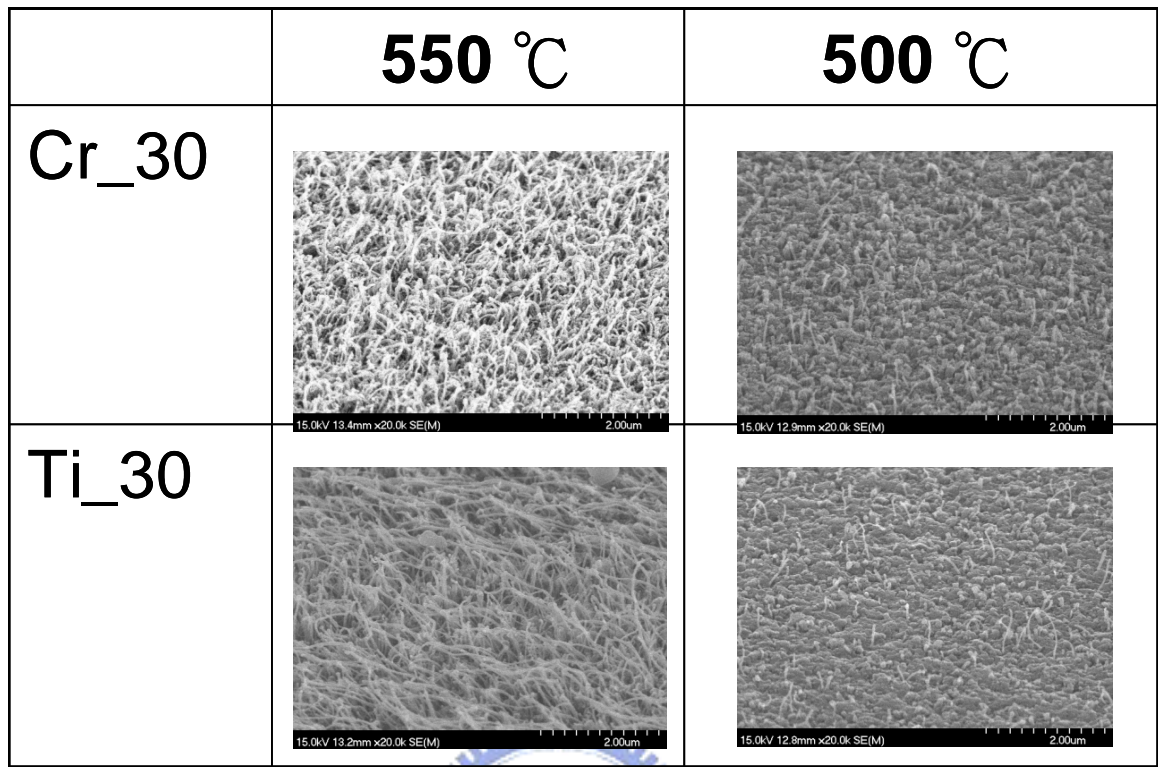


Fig. 3-35 The SEM top views and cross-section images of CNT grow in Exp.G

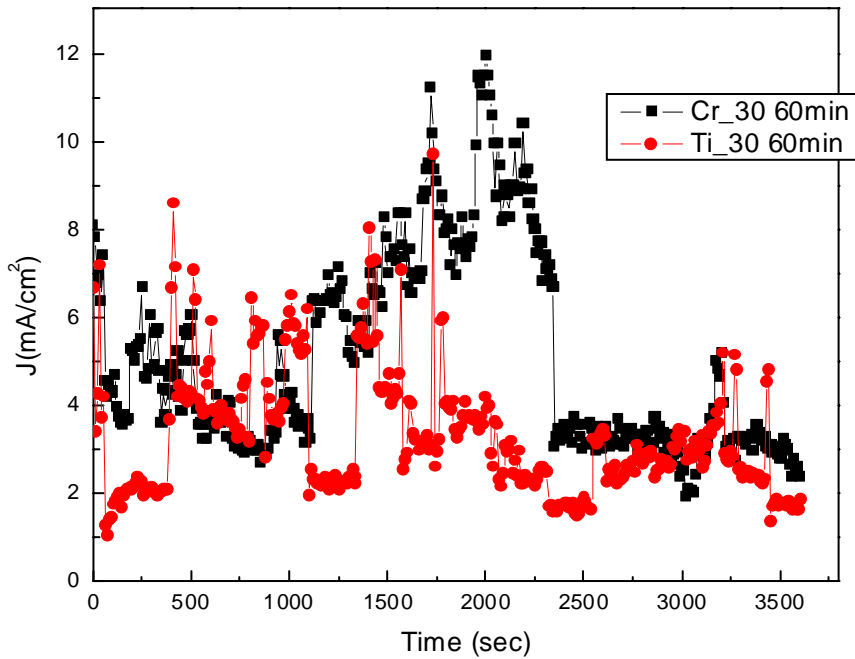
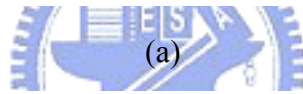
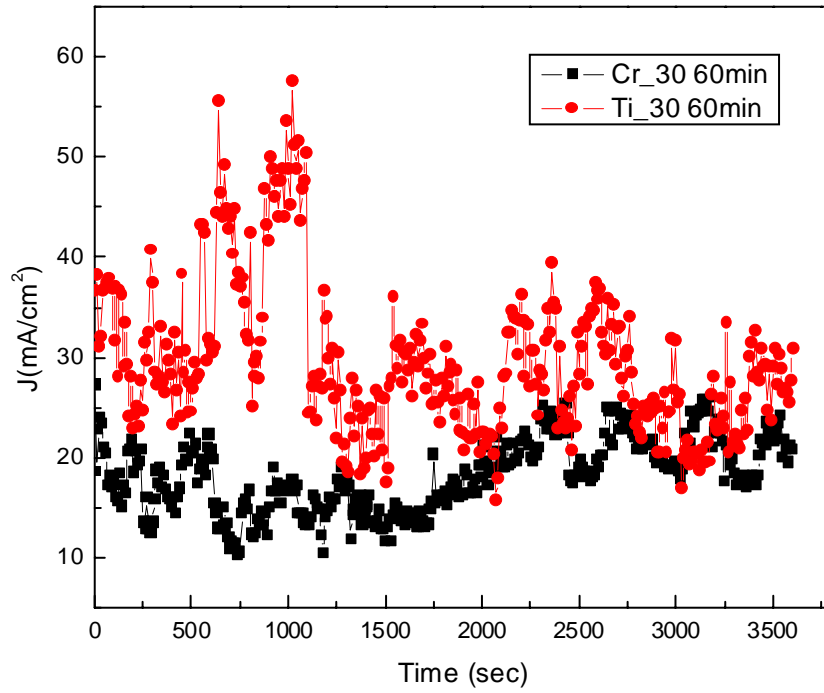
Table 3-13 Stress test in Exp. G , (a) Ti 30 A, and Cr 30 A at 550°C (b) Cr Ti 30 A, and Cr 30 A at 500°C.

(a)

坡	Ti_30	60 min	Cr_30
STD	7.55		3.61
AV(mA/cm ²)	29.63		18.31
C.V	25.48%		19.72%
Final(mA/cm ²)	24.9		20.5

(b)

坡	Ti_30	60 min	Cr_30
STD	1.39		2.30
AV(mA/cm ²)	3.28		5.09
C.V	42.40%		45.22%
Final(mA/cm ²)	2.59		3



(b)

Fig. 3-36 The stress test of Exp.G,(a)at 550°C,(b)at 500°C





	550 °C	500 °C
Ti_30		
Cr_30		

Fig. 3-37 The Luminescent image in Exp. G .

